



This is a repository copy of *Self-assembling structural colour in nature*.

White Rose Research Online URL for this paper:

<https://eprints.whiterose.ac.uk/135421/>

Version: Published Version

Article:

Burg, S. and Parnell, A. orcid.org/0000-0001-8606-8644 (2018) Self-assembling structural colour in nature. *Journal of Physics: Condensed Matter*, 30 (41). 413001. ISSN 0953-8984

<https://doi.org/10.1088/1361-648X/aadc95>

Reuse

This article is distributed under the terms of the Creative Commons Attribution (CC BY) licence. This licence allows you to distribute, remix, tweak, and build upon the work, even commercially, as long as you credit the authors for the original work. More information and the full terms of the licence here:

<https://creativecommons.org/licenses/>

Takedown

If you consider content in White Rose Research Online to be in breach of UK law, please notify us by emailing eprints@whiterose.ac.uk including the URL of the record and the reason for the withdrawal request.



eprints@whiterose.ac.uk
<https://eprints.whiterose.ac.uk/>

TOPICAL REVIEW • OPEN ACCESS

Self-assembling structural colour in nature

To cite this article: Stephanie L Burg and Andrew J Parnell 2018 *J. Phys.: Condens. Matter* **30** 413001

View the [article online](#) for updates and enhancements.

You may also like

- [Photon management for enhanced open-circuit voltage in nanostructured solar cells](#)
S Sandhu, Z Yu and S Fan
- [The influence of the topography and physico-chemical properties of the cuticle surface on the wettability and adhesive properties of the elytra of the dung beetle *Geotrupes stercorarius* \(Coleoptera, Scarabaeidae\)](#)
Mingxia Sun, Esther Appel, Alexander Kovalev et al.
- [Elytra coupling of the ladybird *Coccinella septempunctata* functions as an energy absorber in intentional falls](#)
Jie Zhang, Qiufeng Yuan, Yiling Jiang et al.

Topical Review

Self-assembling structural colour in nature

Stephanie L Burg and Andrew J Parnell 

The Department of Physics and Astronomy, The University of Sheffield, Hicks Building, Western Bank, Sheffield S3 7RH, United Kingdom

E-mail: a.j.parnell@sheffield.ac.uk

Received 17 April 2017, revised 7 August 2018

Accepted for publication 23 August 2018

Published 20 September 2018

**Abstract**

The diversity and vividness of structural colour in the natural world have been recognised as far back as William Hooke in the 17th century. Whilst it is only recently that advances in the field have revealed the elegance and finesse of the physics used to create these effects. In this topical review we will highlight some of the structures and effects responsible for colour in butterfly scales, bird feathers, plants, insects and beetle elytra that have been studied to date. We will discuss the structures responsible and look at similarities and differences in these structures between species. This will be alongside our current understanding of how these are created biologically, how they develop structurally and what control mechanisms nature has at its disposal to control structure formation.

Keywords: photonics, structural colour, biomimetics, bioinspired, phase separation, self assembly

(Some figures may appear in colour only in the online journal)

Introduction

The world around us is highly colourful, and it is somewhat awe inspiring that a large fraction of the colour of everyday animals, insects and plants is produced using structures that are in fact small nanoscale assemblies which selectively reflect certain wavelengths of light [1]. Seminal works [2–5] by a number of researchers have emphasised the importance of *structural colour*—that is, colour that arises not primarily from dyes or pigments, but via diffraction effects from structures with periodic features structured on length scales commensurate with the wavelength of visible light. We are now beginning to understand the structural colour diversity present in the natural world and this review will summarise a small selection of some of these studies. It must be stressed that nature is able to produce structural colour without a high tech factory or a clean room using a series of multi-stage processing steps, as is currently required to produce modern cutting edge man-made photonic

structures and devices. One of the goals of this research area is to use the knowledge and understanding of evolutionary optimised natural structural colour, and incorporate either all or part of existing biological designs into new devices and novel structures, this is often called biomimetic research.

In order to create biomimetic equivalent materials, the crucial question of how these optical nanostructures arise must be comprehensively understood, so that similar assembly mechanisms may be employed industrially. Nature produces these structures via the use of phase separation, minimising free energy, a process we call self-assembly. These structuring and formation mechanisms rely on minimising free energy as well as chemical potentials to drive matter from some initial state to another state based on the interaction of the constituent biological chemical components and molecules. These interactions could be hydrophobic–hydrophilic interactions that are used by lipid like molecules to tune morphology by altering the amphiphilic nature of the templating molecule, depletion attraction forces, or solvent non-solvent effects in the case of spinodal phase separation.

The animal kingdom provides us with some of the most stunning and relatively long-lived eye-catching materials,

 Original content from this work may be used under the terms of the [Creative Commons Attribution 3.0 licence](https://creativecommons.org/licenses/by/3.0/). Any further distribution of this work must maintain attribution to the author(s) and the title of the work, journal citation and DOI.

many of which are still in display in museums and collections around the world. Animals observed in everyday life provide strong variation in the types of structural colour, such as shimmering bright blue of a bluebottle fly, the ornate pattern of a starling, or the subtlety in colour of a Eurasian blue tit's crown feathers [6]. More often than not the structural colour discussion begins with the flamboyant feather display of the male peacock (*Pavo cristatus*) [7] (which can be seen in figures 1 and 2(a)). This has historically been seen as the archetypal example of structural colour throughout history, as can be seen from figure 1, and has intrigued and mystified numerous generations [8].

Structural colour in peacocks and pheasants was observed and studied by a number of scientific luminaries; Robert Hooke [9], Sir Isaac Newton [10] and Sir Chandrasekhara Raman [11].

To be clear, there are many other examples beyond these particular animals. However, this work will examine a carefully selected range of morphologies used to produce structural colour, which span many different animal species [12] and living systems including plants, with great variety in the possible colours [13]. We will see that there are indeed some general trends in the kinds of morphologies and structures. It is worth noting that more often than not the structures are used in concert with pigmentary absorbing materials [14–17] as either a basal layer to enhance contrast or to absorb a particular part of the optical spectrum.

1. The physical mechanisms and optical effects by which colour can be produced

Biological photonic nanostructures depend on the presence of a refractive index contrast between materials, however nature does not commonly use high refractive inorganic materials, as is the case for man made photonic materials such as tantalum pentoxide (Ta_2O_5), which has a refractive index, n , of 2.275. Instead nature has at its disposal biological polymers, like beta-keratin, chitin and collagen. Chitin is a common organic polymer that is structurally similar to cellulose. All of these are essentially low refractive index materials with values close to ~ 1.5 [18], the key to making biological photonic structures is that nature uses air voids as the other phase giving a relatively large refractive index difference ($\Delta n \sim 0.5$). An alternative approach to this is to use melanin with a refractive index ~ 2 and beta-keratin ~ 1.5 again giving a similar difference in the refractive index. A review of some of the many ways in which it is possible to characterise biologically structurally coloured materials (SEM, FIBSEM, TEM, AFM) and also measure their optical properties (spectrophotometry, integrating sphere, imaging scatterometry [19] and reflectometry) is detailed in the review by Vukusic *et al* [20]. These experimental techniques have been used to elucidate the structures and effects that will be discussed in this review article. The following sections will detail the types of optical structures that have been achieved in nature, which are diverse [21]. These range from being strongly viewing angle dependent, highly iridescent



Figure 1. The peacock stage as a symbol of one of the steps in alchemy when the contents of the vessel turn from an oily black colour to vividly iridescent, taken from a medieval text on alchemy [8]. This Splendor Solis 16 venus peacocks tail image has been obtained by the authors from the Wikimedia website (https://commons.wikimedia.org/wiki/File:Splendor_Solis_16_venus_peacocks_tail.jpg), where it is stated to have been released into the public domain. It is included within this article on that basis.

structures through to isotropic colour, which can be observed independently of viewing angle, i.e. constant hue.

An in-depth discussion and summary of the reflection of light via thin film interference [22], multi layer interference, chirped multilayers, coherent reflectors and the concepts of photonic crystals are discussed elsewhere [23]. But it is worth briefly highlighting the underlying physics of these materials, mainly that they use constructive interference and often multiple interfaces structured on lengthscales comparable to the wavelength of light [24].

One of the simplest examples of an assembly, which will produce a structural colour, is a thin film. A thin film causes what is known as thin film interference. Incident light strikes the thin film, which has some thickness d , at an angle θ_a and the light is both reflected and refracted at the top interface of the film. The light is refracted at an angle of θ_b and when

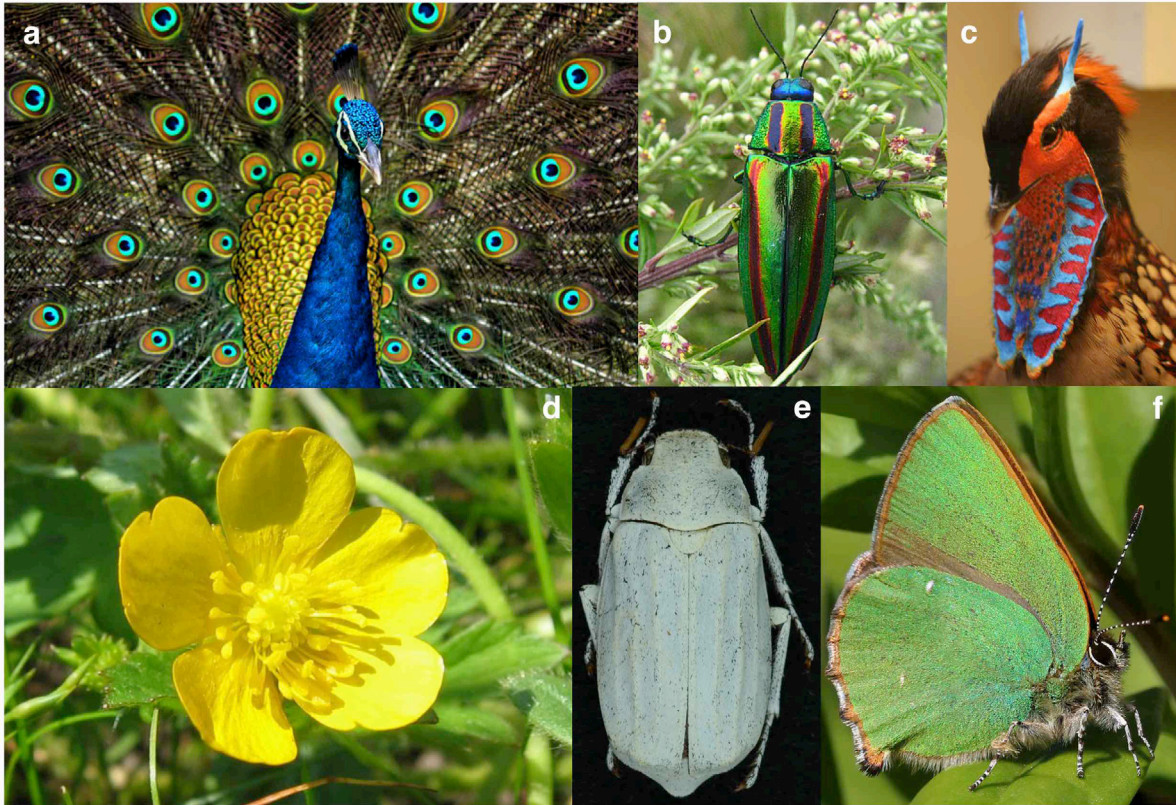


Figure 2. (a) Male peacock (*Pavo cristatus*). This Peacock Plumage image has been obtained by the authors from the Wikimedia website (https://upload.wikimedia.org/wikipedia/commons/c/c5/Peacock_Plumage.jpg) where it was made available by Jatin Sindhu under a CC BY-SA 4.0 licence. It is included within this article on that basis. It is attributed to Jatin Sindhu. (b) A Japanese jewel beetle (*Chrysochroa fulgidissima*). This *Chrysochroa fulgidissima* (Tamamushi) In Nature image ([https://commons.wikimedia.org/wiki/File:Chrysochroa_fulgidissima_\(Tamamushi\)_In_Nature.PNG](https://commons.wikimedia.org/wiki/File:Chrysochroa_fulgidissima_(Tamamushi)_In_Nature.PNG)) has been obtained by the authors from the Wikimedia website, where it is stated to have been released into the public domain. It is included within this article on that basis. (c) Cabot's tragopan (*Tragopan caboti*). This Sekretär Vogel image has been obtained by the authors from the Wikimedia website (https://commons.wikimedia.org/wiki/File:Sekret%C3%A4r_Vogel.JPG), where it is stated to have been released into the public domain. It is included within this article on that basis. (d) Buttercup (*Ranunculus repens*). This *Ranunculus repens* bluete image has been obtained by the authors from the Wikimedia website (https://commons.wikimedia.org/wiki/File:Ranunculus_repens_bluete.jpeg) where it was made available (by Fabelfroeh) under a CC BY 3.0 licence. It is included within this article on that basis. It is attributed to Kristian Peters. (e) *Cyphochilus insulans*. (f) Green hairstreak (*Callophrys rubi*). This Green hairstreak (*Callophrys rubi*) 3 image has been obtained by the authors from the Wikipedia website ([https://en.wikipedia.org/wiki/File:Green_hairstreak_\(Callophrys_rubi\)_3.jpg](https://en.wikipedia.org/wiki/File:Green_hairstreak_(Callophrys_rubi)_3.jpg)) where it was made available by Charles J Sharp under a CC BY 4.0 licence. It is included within this article on that basis. It is attributed to Charles J Sharp.

the refracted light encounters the bottom interface the light is again reflected and refracted. The primary $m = 1$ order reflectance can be calculated using equation (1)

$$2n_b b \cos \theta_b = m\lambda. \quad (1)$$

The refracted light from the bottom interface exits the film and the reflected light will again encounter the top interface of the film to be again reflected and refracted. If the thin film is highly reflective then this process can continue as the light bounces back and forth inside the film. The reflected light waves coming off the top of the film will interfere through the principle of superposition. A simulation for a series of different thin films of chitin is shown in figure 3(a), showing how subtle changes in the film thickness can allow the peak reflectance to be moved across the visible spectrum. One of the most striking features of thin-film diffraction is the dependence of the overall reflectance on the angle of incidence.

Examples of thin film interference are found in numerous butterflies such as the *Aglais io* [28] and recently in the palm

borer moth *Paysandisia archon* [25] showing this is generic across butterflies and moths.

To increase the reflected intensity from a structure without increasing the refractive index involves stacking multiple alternating layers together. Then the light that exits the very top surface of the multilayer stack will then again interfere with one another to give the final reflectance. The optical path difference (OPD) of the light exciting the stack will be the sum of the OPD from layer a and layer b and the condition for constructive inference from single a - b pair is given by equation (2), where m is again an integer. The reflectivity of a multilayer structure was first derived in 1917 by Lord Rayleigh. Since then many numerical methods have been developed such as the transfer matrix method, which is the method implemented in the TMM Python package [27] and was used to simulate figures 3(c)–(e)

$$2(n_a d_a \cos \theta_a + n_b d_b \cos \theta_b) = m\lambda. \quad (2)$$

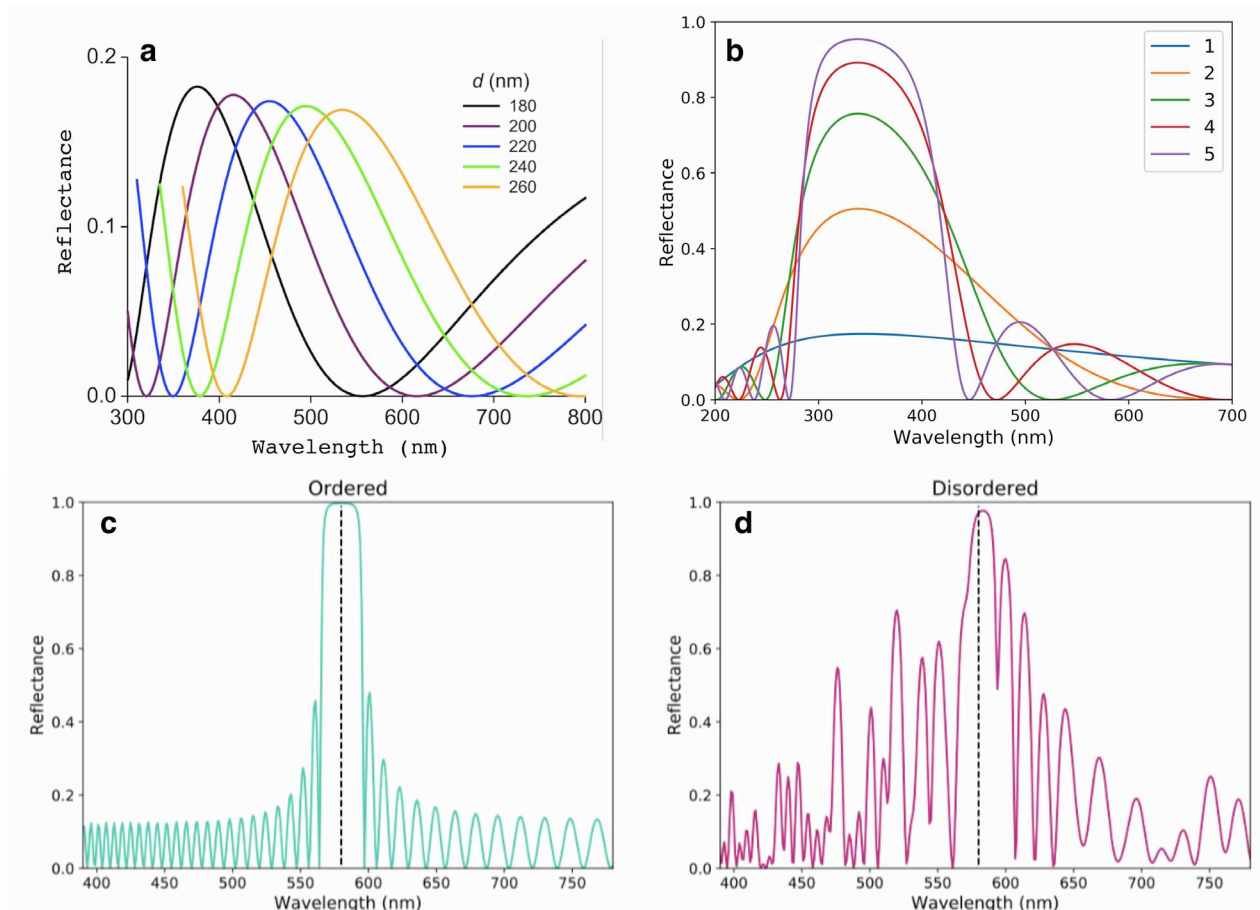


Figure 3. (a) The reflected intensity from normally illuminated chitin thin film layers having thickness in the range 180 nm–260 nm. Reproduced from [25]. [CC BY 4.0](#). (b) Simulation of the male butterfly *Eurema lisa* optical multilayer with a periodic stack of 55 nm chitin and 83 nm for the air space [26], simulation performed using the python package written by Steven Byrnes [27]. Parts (c) and (d) are the reflectance intensity for a 1D photonic crystal with 50 layers (n of 1.5 and 1.4, both layers are 100 nm thick), with (c) having perfect layer repeat thicknesses and (d) having a degree of disorder in the thickness.

The first thing immediately obvious from multilayer interference is the strong sharpening in the reflectance peak with respect to increasing the number of layers. This means that multilayer microstructures are strongly vivid in colour and exhibit strong iridescence. Additionally, as the number of layers increases from one, to two, to three layers there is a steep increase in the maximum reflectance. However, after five layers the gain in reflectance for each added layer begins to drop off and by nine layers the maximum reflectance reaches unity with the intensity of the incident light at 1. This means that by using just a few layers a biopolymer such as chitin or beta-keratin with a relatively low refractive index, it is possible to achieve highly reflective and strongly coloured materials.

Photonic crystals refer to a material in which the refractive index varies periodically under the condition that the period over-which the refractive changes must be on the order of the wavelengths of visible light. In a sense photonic crystals have already been introduced as the multilayer stacks of thin films that are often referred to as 1D photonic crystals. However, photonic crystals are not constrained to stacks of thin films and can also be made from periodic structures of rods or spheres. The way that light interferes when it encounters a photonic crystal causes what is known as a photonic band gap,

these are wavelengths of light that cannot propagate in the material and are reflected out. In the reflectance plots for the multilayer film stacks in figure 3(b) the photonic band gap is the centre of the reflectance peak.

Typically, photonic crystals exhibit well-defined long-range order. However, it is possible to recover some of the reflectance properties of a photonic crystal even when the long-range order has been disrupted. To demonstrate this the multilayer film is revisited and figures 3(c) and (d) shows the reflected intensity for a stack of 50 layers of a material with a refractive index of 1.5 embedded in a material with a refractive index of 1.4. The thickness of both layers was fixed at 100 nm and the incident light was normal to the surface. Disorder was introduced into this system by allowing the layer with the refractive index of 1.4 to vary a randomly by $100 \text{ nm} \pm \delta$ where δ is a randomly selected percent change between -35% and 35% of the layer thickness.

For the perfect uniform structure the reflectance shows a clear band gap at 580 nm highlighted by the dashed line in figure 3(c). The reflectance of the 1D photonic crystal in (d) is much less uniform, as a degree of disorder has been added by varying the thickness of the layers. The reflectance no longer shows evidence of a band gap, but does have a notional peak

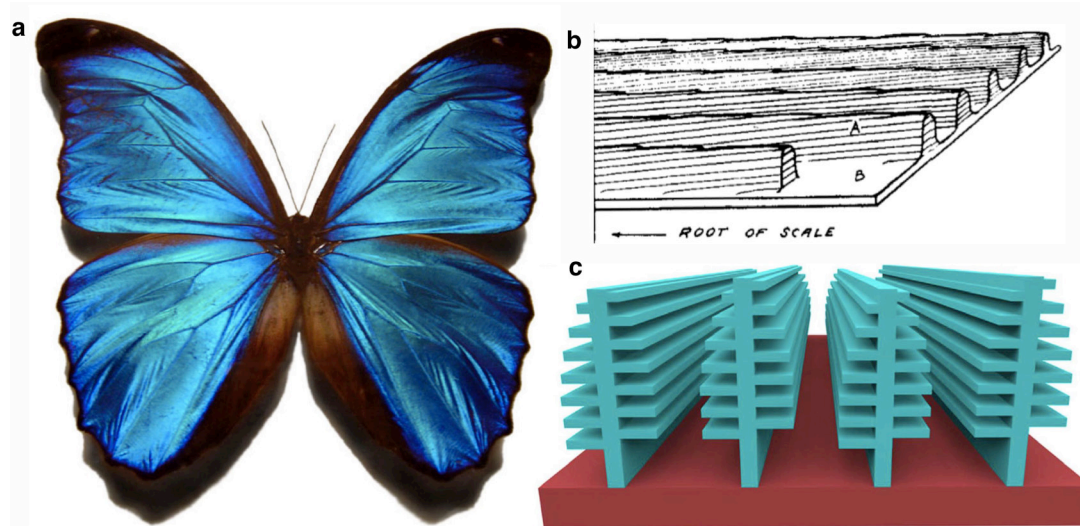


Figure 4. A diagram showing the optical nanostructure found on the surface of the scales of a Morpho butterfly. (a) Photograph of a blue Morpho (*Morpho menelaus*) butterfly. This Blue morpho butterfly image has been obtained by the authors from the Wikimedia website (https://commons.wikimedia.org/wiki/File:Blue_morpho_butterfly.jpg) where it was made available by Fanghong under a CC BY 3.0 licence. It is included within this article on that basis. It is attributed to Gregory Phillips. (b) The original drawing by Dr Clyde Mason of the *Morpho* surface scale features taken from [30] where B is the basal layer, A are the longitudinal veins. The surface is made up of inclined multiple thin films—and the origin of the structural colour. Reprinted with permission from [30]. Copyright 1927 American Chemical Society. (c) A is a schematic showing the Christmas tree like shape with tapered and off-set lamellae composed of alternating chitin and air. Reproduced from [32]. CC BY 4.0.

in reflectance near the band gap of figure 3(c) marked again by a dashed line.

The topic of coherent quasi-periodic reflectors will be covered in detail in later sections 3.3, 4.2 and 4.3.

2. Butterfly structural colour

2.1. Surface structures—Bragg mirrors

The different optical structures found in the numerous species of butterflies range from ridge reflectors like those found in the *Morpho didius*, as shown in figure 4, to structures which are located internally inside the individual butterfly scales.

A detailed description of the state of the art in terms of our understanding of *Morpho* type ridge reflectors can be found elsewhere [13, 29]. These are highly regular structures, which reflect nearly 75% of the incident blue light. An example of a *Morpho* is shown in figure 4, along with one of the original sketches from Dr Clyde Mason [30], and a vertical rendering showing the offsetting of the ridges. It has been shown that the top layer of cover scales and the lower ground scales work in a cooperative manner, with the cover scale acting as an optical diffuser. This is important as the vivid blue colour effect can be seen over a wider angular range [31].

Whilst human vision makes us aware of the eye-catching iridescent colour found in the *Morpho* family of butterflies, there are more inconspicuous examples to be found in other butterfly families, like *Pieridae* [26]. Male and female butterflies of *Eurema lisa* have been shown to exhibit sexual dimorphism in colouration, which is cryptic to human vision but not to each other, as some insects are readily able to see in the UV. Male *Eurema lisa* possess a surface decoration of structured lamellae, very much like that seen in *Morpho* butterflies,

but with a reflection in the UV peaked near ~ 350 nm, having an alternating lamellar structure of 55 nm of chitin and 83 nm for the air space. When the component refractive index is accounted for they exhibit a comparable optical thickness, chitin 88 nm and air 83 nm, this multilayer structure is simulated in figure 3(b) for an increasing number of repeat pairs. Ghiradella highlighted that even though there are strong differences in the phylogeny between *Morpho* and *Pieridae* they have both converged on a strikingly similar solution to generate structural colour. Showing that there is great flexibility and plasticity in the arthropod integument, and convergence to an optimal design is possible.

Colour mixing, most often using a combination of pigment and structural colour is a recurring theme and will be mentioned numerous times in this review, this approach gives great flexibility and variability. Colour mixing has been effectively used by the green butterfly *Papilio palinurus* where spatial arrangement of different wavelength reflecting multilayers (yellow and blue) allows averaging by vision to produce a green colour [2]. This understanding has been confirmed by the production of an analogous synthetic concave multilayer structure, using the *Papilio blumei* as the design structure [33]. Production of a synthetic version required a number of stages, which include; colloidal self-assembly, electro-plating, sputtering of a multilayer stack, this was using inorganic materials Al_2O_3 and TiO_2 to create the multilayer. This shows how optical design from nature can be used to create photonic devices and technologies with comparable optical effects.

2.2. Lower lamina reflectors

Another way in which it is possible to create structural colour is from thin films at the base of the butterfly scale, commonly

termed lower lamina reflectors (highlighted earlier in section 1, see figure 3(a)). One such example of a structure can be found in the eyespot region of the peacock butterfly (*Aglais io*) [28]. Measurements on a single scale gave reflectance peaked at ~430 nm, optically modelling a selection of thin film reflectors of varying thicknesses showed the lower lamina was around 200 nm thick. When the layer was reflecting blue there was little or no pigment present. The situation becomes more complex with the addition of pigment, the colour becomes a composite of the colour reflected from the lower lamina and the selective absorption from the pigment. Also scale stacking and arrangement becomes important when trying to understand the total interaction of the different components.

3. Beetle structural colour

Beetles (*Coleoptera*) show a diverse range of structural colours; to date only a very small fraction of the near 400 000 species of beetle have been studied optically and structurally. This is a huge resource that will certainly contain new and interesting optical phenomena that can be investigated, optically modelled and understood. A more complete review of some of the existing beetle optical structures can be found elsewhere [34]. We will however show a few examples of the possible ways in which beetles use structural colour in the elytra, surface hairs/features and other parts of their body.

3.1. Multilayer reflectors

There are many different types of insect, a large fraction of which contain one dimensional photonic crystals, often termed Bragg stacks, this is responsible for the colour effect observed in case of the Japanese jewel beetle *Chrysochroa fulgidissima*—shown in figure 2(b). These are structures in which there is a repeating alteration of the refractive index, in the beetle case these do not have the air space like butterflies, but instead tend to be solid layers.

3.2. Three dimensional photonic crystal structures

There are numerous examples of fully three dimensional crystalline domain structures in insects and beetles that extend over large volumes. We will focus our attention on a particular well studied photonic crystal structure [35] that gives rise to a green with a strikingly wide viewing angle. This kind of structure has been found in a number of species and is presumably used as either a warning signal to avian predators or a sexual display of mate fitness. We are now beginning to understand how this structure forms (see later section 6.3). In one of the earliest works to study the green scales of the emerald-patched cattleheart butterfly (*Parides sesostris*—shown in figure 5(a)) Ghiradella [36] observed that the inner space of the butterfly scale is occupied by micron sized photonic crystal grains. In subsequent work Ghiradella studied the green hairstreak (*Callophys rubi*) which possesses similar green internally structured scales. The nano-optical structure fills the volume normally occupied by the trabeculae and pigments granules,

Ghiradella concluded that the structure was a series of closed packed spheres [37], where self-assembly drives the ordering due to the requirement to minimise the free surface area. The structure observed has been characterized as a gyroid morphology, gyroid structures are termed minimal surfaces as mathematically they represent a structure with minimal area whilst still providing full interconnectivity. They are well known structures found in surfactant science and in polymer block copolymer morphologies.

On top of this distinctive nano-structure are long ridges (see figure 5(d)), which Vukusic *et al* [21] mentioned that this as an elegant way of incorporating a wide viewing angle, by enclosing the structure within the scale and orienting the small crystal domains at different orientations to one another. Poladian *et al* [38] went further in analysing these structures and noted that the ridge structure on top of the gyroid domains is of a similar thickness for *Parides sesostris*. By examining the optical reflectance from above and below and altering the angle of incidence, they saw that the reflectance from above had a reflectance maximum that varies gradually from 550 nm to 525 nm upon changing the viewing angle. Whereas from below and without the benefit of the thick ridge layer, the gyroid structure has abrupt and rapid changes in the reflectance maximum down to ~500 nm, showing that this ridge layer lessens the angular viewing dependence. The strong iridescence exhibited from the underside, can be seen clearly in figure 5(b), where there is a large difference in the reflected light intensity, with the gyroid crystal surface giving about three times more reflected intensity than the gyroid surface with the ridge structure. They used adhesive tape to remove the ridge layer and saw by optical microscopy the striking difference in colour with and without the ridge layer. Possible explanations for how these ridge structures achieve a broadening of the angular colour are by acting as a collimating structure or by helping to scatter and randomise the angles for the incoming and reflected light.

Wilts *et al* [39] also performed studies on the scales of *Parides sesostris* through the optical characterization of the reflectance from above and below, using imaging scatterometry [19] to examine the scattering as a function of angle. Using fluorescence microscopy, they were able to ascertain that the upper ridge layer contains an absorbing pigment, which absorbs below 450 nm. By constructing the photonic band structure for the gyroid and overplotting the range of the pigment absorption they were able to explain how the *Parides sesostris* is able to produce an angle independent structural green, by damping the reflected colour (by absorption) and restricting the range of reflected wavelength from 450 nm to 600 nm.

Michielsen *et al* [40] performed a comprehensive survey for a number of *Papilionidae* butterflies (including *Parides sesostris*) as well as *Lycaenidae* (*Callophys rubi*—see figure 2(f)), *Mitoura gryneus* amongst others. Using a series of existing electron microscopy images they were able to use analytical modelling and simulations to generate 3D virtual structures. They concluded, based on comparison of optical modelling, that the measured butterfly scale 3D structures in the butterfly inner scales are filled with gyroid structures. They were also able to show that a number of other specimens

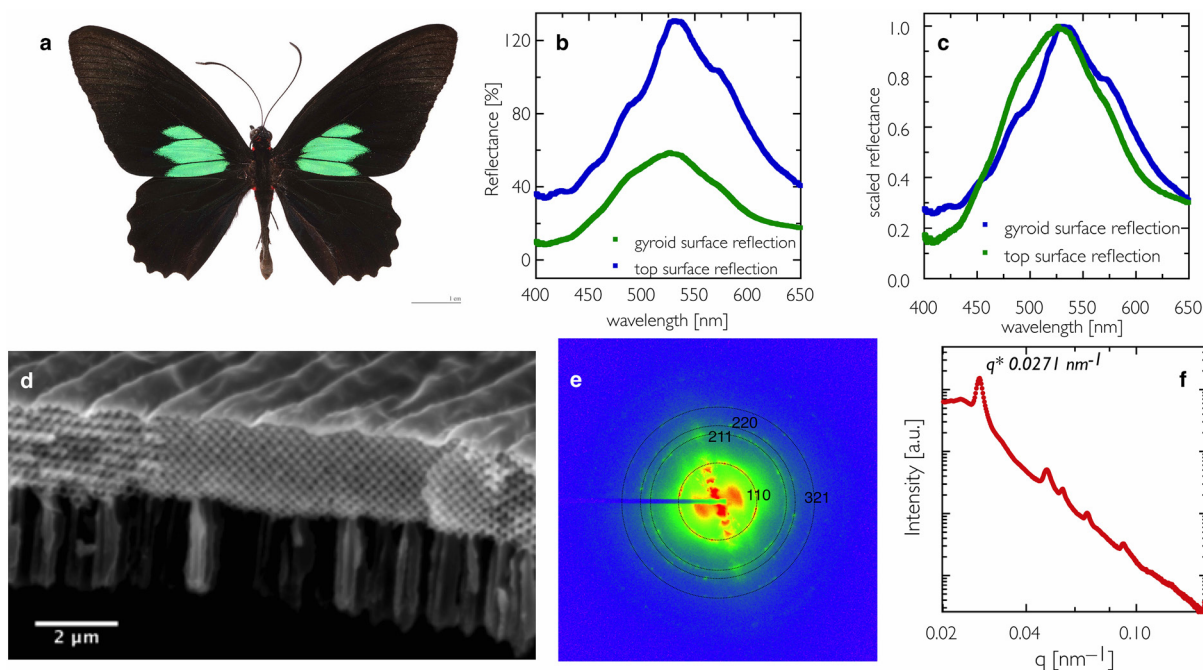


Figure 5. Structural and optical characterisation of an emerald-patched cattleheart butterfly (*Parides sesostris*). (a) Photograph of a *Parides sesostris*. This *Parides sesostris* image (https://commons.wikimedia.org/wiki/File:Parides_sesostris_MHNT_dos.jpg) has been obtained by the authors from the Wikimedia website where it was made available by Archaeodontosaurus under a CC BY 4.0 licence. It is included within this article on that basis. It is attributed to Didier Descouens. (b) Optical reflectance measurements taken at normal incidence of the top surface (green) and bottom surface, showing the big difference in the reflected intensity. In (c) the reflectance peaks have been scaled to enable comparison of the spectral shape. (d) An SEM cross section of a *Parides sesostris* scale, (the scale is upside down i.e. light would normally be incident from below). (e), (f) SAXS data taken in transmission. (e) The two dimensional scattering pattern and reflections that are indexed showing that this structure corresponds to a gyroid structure and (f) the radial integration showing the peak positions in reciprocal q space.

can all be categorised as a family of gyroid structures of varying lattice structure and filling fraction.

Saranathan *et al* [41] used small angle x-ray scattering (SAXS) and indexing of the strong reflection peaks to determine the lattice parameter, a , for the green butterfly regions of the *Parides sesostris* (amongst a number of other *Papilionidae* and *Lycaenidae* butterflies) as 329 nm. This confirmed unambiguously using crystallography that they are indeed three dimensional gyroid structures, based on the position of the crystal reflections in q space. They were also able to estimate the average domain size of the gyroid crystal grains at 4.5 μm , using a Scherrer type peak analysis. Our own SAXS data showing the two dimensional scattering pattern and a radial integration for a *Parides sesostris* are shown in figures 5(e) and (f). Performing the same calculation we measure a very similar lattice parameter value to that measured in [41], ours being 327 ± 2 nm, showing the robustness of scattering as a means to determine structure.

3.3. White structural colour

Gadow was amongst the first [42] to correctly articulate the many ways in which it is possible to create white using structure, Mason [43] also correctly identified that the majority of structural whites rely on multi-lengthscale scattering systems. These are predominantly two-phase porous materials in which the pores or voided spaces contain air, whilst the other phase

is a solid material comprised of a stable biopolymer such as chitin or beta-keratin. Dyck also found evidence for a structural white in the feathers of ptarmigans and postulated that it may help improve heat retention, particularly important for arctic animals [44].

One of the most studied classes of structural white materials in nature has been that of the ultra-white insects, primarily due to their impressive whiteness and opacifying ability. This class of beetles contains amongst them the *Lepidiota stigma* and the *Cyphochilus*. The first scientific paper examining the origin of the supreme whiteness of these beetles was published over ten years ago by Vukusic *et al* [3] who studied the internal structure of these white scales using electron microscopy. They were able to show how the scales of the *Cyphochilus* beetle at just 5 μm in thickness (although later studies it put this thickness nearer 10 μm), possess a similar whiteness and optical brightness to those of synthetic systems two orders of magnitude thicker.

The internal structure of a sectioned scale in cross section can be seen in figure 6, it clearly shows that the scales are composed of a network of chitin filaments with air spaces. The top surface contains some features reminiscent of anti reflection coatings, but this has yet to be confirmed via optical modelling. Two-dimensional fast Fourier transform analysis of the TEM images revealed no evidence of periodicity. A comparison of the optical diffraction pattern for a single scale with those of the Fourier transforms of the TEM images

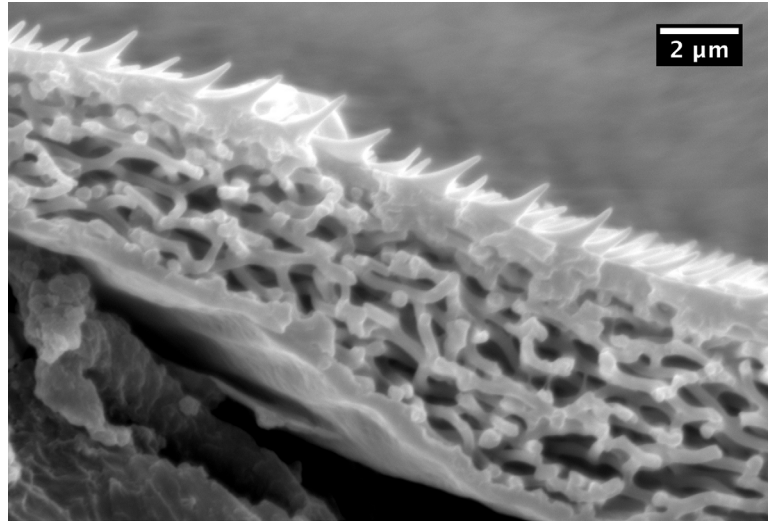


Figure 6. A cross sectional scanning electron microscopy (SEM) image of the internal structure of an ultra white *Cyphochilus* beetle scale. The regular spike features on the top surface of the scale are either an antireflective coating type structure or a structure that makes the beetle displace water by being strongly hydrophobic, or possibly serves both purposes.

confirmed that the internal disordered network is the source of the scales impressive optical scattering. The *Cyphochilus* scales immediately gained further attention and in Hallam *et al* [45] they took inspiration from the internal scale structure to show how the light scattering ability of paper coatings could be improved. This work emphasized that the key variables that allow the *Cyphochilus* to scatter light so effectively are the filament width, the spacing between filaments, and the packing density or the volume fraction chitin to air within the scales. Based on the analysis of the TEM scale sections they reported chitin filaments with a thickness of 250 ± 50 nm and a mean spacing between them of 600 ± 260 nm.

In 2011, a paper by Luke *et al* [46] attempted to further quantify the structural parameters which dominate and control the optical scattering. It also introduced the *Lepidiotia stigma* and *Calothyrsa margaritifera* as further examples of beetles with ultra white scales, using a two-phase network of chitin and air. Again, through detailed analysis of SEM and TEM images the authors also reported filling fractions for the scales of *Cyphochilus* (0.68 ± 0.07), *C. margaritifera* (0.48 ± 0.03) and *L. stigma* scales (0.56 ± 0.08). The study also converted the TEM images of the scales to two-dimensional slices and imported them directly into a commercial optical modelling package allowing the authors to investigate how varying the structural parameters (scattering centre size, spacing, and volume fraction) of the scales affected their ability to scatter light. Their conclusion was that broadband whites tread a fine line in parameter space to provide efficient white light scattering whilst resisting optical crowding. The *Cyphochilus* was most effective broadband scattering structure per unit thickness, due to it having a more optimized filament thickness. These white scattering scale structures must therefore be optimised presumably via evolution to perform this function.

Burresi *et al* [47] used time resolved optical measurements to study the confinement and propagation of light in the ultra-white scales of *Cyphochilus* and *Lepidiotia stigma*. Using a pump probe type ultrafast optical spectroscopy setup they were

able to measure the residence lifetime of the transmitted light in the scales, this gave values of 140 fs and 210 fs respectively, for *Cyphochilus* and *Lepidiotia stigma*. This is much greater than would be expected for single site scattering in the scales which would produce delays on the timescale of a few \sim fs. Their conclusion was that the scales act as strongly scattering optical systems where the mechanism is dominated significantly by multiple scattering. Their values of scale filling fraction, extracted from their optical modelling simulations, gave values for *Cyphochilus* of (0.61 ± 0.02) and *Lepidiotia stigma* (0.50 ± 0.03), which are in reasonable agreement with the values from previous work [46]. What was strongly distinct in this work was that they concluded that the white beetles scales use a dense air chitin network to create a strongly anisotropic disordered medium. From the SEM images of their sectioned scales data the authors stated that, ‘the elongated chitin elements that constitute the network are mainly oriented parallel to the scale surface’. This conclusion was expanded on with further optical experiments in Cortese *et al* [48] where they examined the shape of the light transmission profile through the scale, this enabled information on the light transport through the scale to be retrieved, principally the mean free transport of the scale internal structure. Using a diffusion model they found it possible to calculate the transport mean free path l_t , this is a measure of the average distance light travels before being scattered, so smaller values mean the structure is much more effective at randomising the impinging light.

Comparing the values of l_t , they saw a large difference in light transport between the different orientations of the scale; principally light scattering was much stronger in the direction normal to the scale surface ($l_t \sim 1.2 \mu\text{m}$). This is at the expense of scattering in the plane of the scale ($l_t \sim 4.6 \mu\text{m}$), so reducing the omnidirectional reflectivity of the scales.

Wilts *et al* [49] realised that one of the problems with electron microscopy investigations of biological structures is that it can create distortion or bring about a volume change in the material under investigation. The resin used to embed

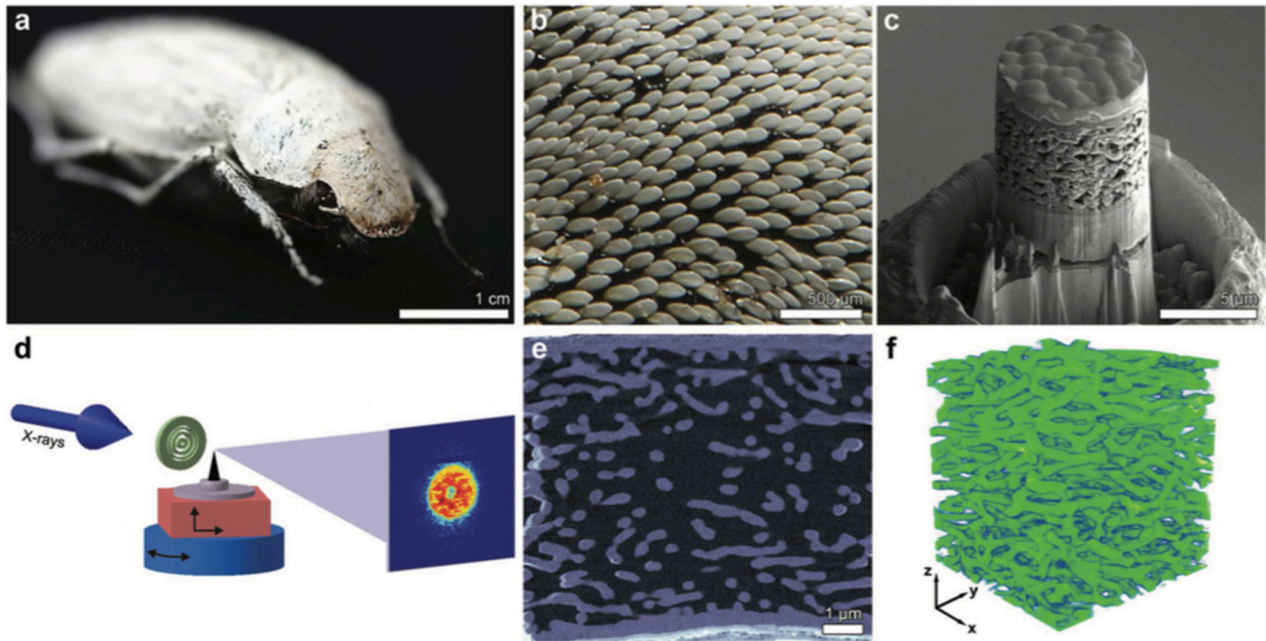


Figure 7. An x-ray nano-tomography study of the ultra white scales of the beetle *Cyphochilus*. (a) An optical image of a *Cyphochilus* specimen, (b) a light microscopy image of the scale decoration on the surface of the beetle's elytra. (c) A focussed ion beam prepared region from the centre of an individual *Cyphochilus* scale, imaged using SEM, (d) shows a schematic representation of the x-ray nanotomography setup used to image the internal nanostructure of the region in (c). Briefly the sample is scanned and rotated through the beam (indicated by arrows) while recording the diffraction pattern. (e) An individual high-resolution tomographic slice used to reconstruct the full 3D volume and (f) a three dimensional volume reconstruction of the inner structure of a beetle wing scale of sides $7\ \mu\text{m}$ acquired using cryo-tomography. Reproduced from [49]. CC BY 4.0.

materials has a volume change on curing and there are also complications when sectioning thin tens of nanometre thick slices. To overcome these problems their recent study used the relatively new technique of x-ray tomography to measure a $\sim 350\ \mu\text{m}^3$ cube ($7\ \mu\text{m} \times 7\ \mu\text{m} \times 7\ \mu\text{m}$) of a *Cyphochilus* scale with a resolution of 28 nm. This is a very powerful technique as it can give a full 3D volume of a material on the nanoscale. Figure 7 shows the various stages in the preparation of the sample from excavation of a portion from within an individual scale to mounting on a suitable substrate. The measurement process involves collecting x-ray patterns at numerous rotations and focal distances. This is all reconstructed to produce a full 3D scale measure volume, shown in figure 6(f). This is made up of individual slices like the one in figure 6(e), with 28 nm resolution.

This optical probe cube of *Cyphochilus* scale has a chitin volume fraction of 0.45 ± 0.06 , so somewhat lower than the values measured using conventional TEM image slices, approaching $\sim 30\%$ lower filling fraction than the values measured previously. This sample cube was modelled to simulate its optical properties using finite difference time domain (FDTD) simulations, having the cube as a 3D matrix *in silico* allowed the filling fraction, refractive index, scaling, stretch and compression to be manipulated to model the light transport from the probe volume. They were able to show that there is a difference in the reflection from the scale structure parallel to the surface of the scale (0.5) and perpendicular (0.65), so again observing the anisotropy described in the previous studies. Interestingly they saw an increase in the reflectance (0.69) perpendicular to the scale surface upon stretching the

scale, and thereby making it more isotropic. Their conclusion was that the white beetle scale had been optimised to create a lightweight broadband reflector using the minimal amount of material, the authors speculated that the scale is grown in a very similar way to the butterfly scale structures mentioned earlier, but that this requires further study to understand this process and so understand the developmental stages leading to this structure.

4. Avian structural colour

The study of structural colour from bird feathers has been a remarkably rich area of structural colour research and has provided insight into many possible ways in which nature is able to produce biological photonic structures. The fact that feathers maintain their colour long after animal death makes them suitable for a number of different types of investigation; from optical spectroscopy to examine the absorption spectra of pigmentary carotenoids [15], through Raman chemical fingerprinting of the carotenoids [50], also structural determination from electron microscopy [51] and increasingly using small angle x-ray scattering [52].

4.1. Iridescent peacock and pigeon feathers

The work of Mason [53] rightly focused in on the most striking characteristic of this class of feathers, that is their iridescence. These structures exhibit a visually stunning metallic like lustre and some for example, appear purple at normal incidence

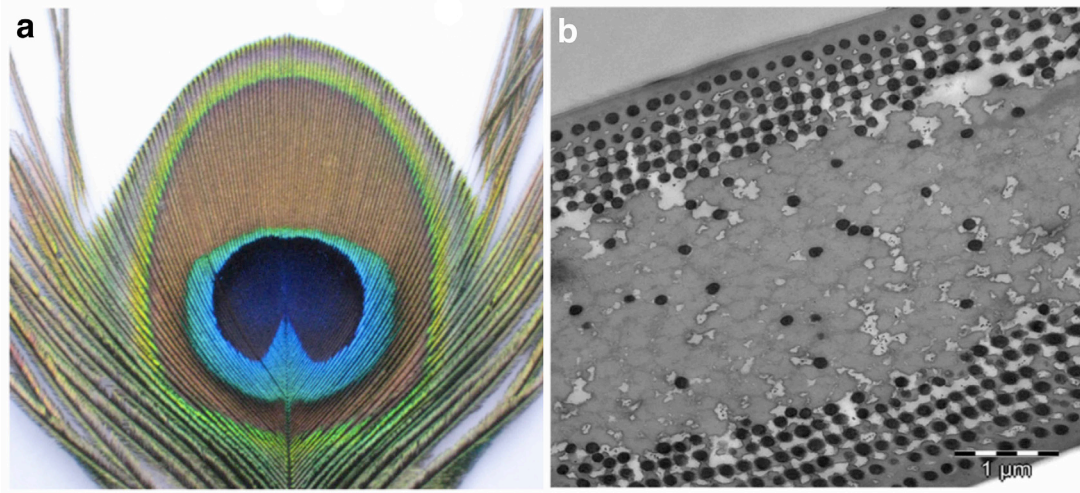


Figure 8. Male peacock. (a) Macroscopic photo of one of the tail feathers and (b) a TEM cross section of a barbule. Reproduced from [55]. CC BY 4.0.

and proceed through to red, yellow and then green as the angle is reduced to near grazing incidence. Mason correctly identified that the colour is located in the barbules of feathers and he performed analysis on cross-sections of peacock feather barbules. Figure 8(a) shows a macroscopic image of a peacock feather and a TEM cross section showing the square optical lattice responsible for the iridescence in figure 8(b). Again it is important to take into account the macroscopic curvature and architecture, which helps to achieve a wide angular viewing range [54].

Nakamura *et al* [56] examined pigeon feathers from the rock dove (*Columba livia*) and found that for the iridescent barbules the colour was determined by the thickness of the cortex which caused the effect via thin-film interference. This gives rise to higher order interference peaks that are situated close to one another in the optical spectrum. For instance a green reflecting patch has reflection peaks near 437 nm, 554 nm and a further higher order peak near 740 nm (outside the visual spectrum). The thickness of the green cortex layer was measured using cross sectional SEM to be between 600–700 nm in thickness. A purple feather coloured was found to be slightly thinner with a cortex thickness between 480–580 nm.

Eliason *et al* [57] studied in detail the structure of a number of iridescent duck wing patches from dabbling ducks, and focussed their attention on the colourful speculum patch present on the secondary flight feathers. Analysis of the barbule nanostructure via TEM showed that the colour was produced using a hexagonally close packed two dimensional array of melanosome rods which are protected beneath a thin keratin cortex outer layer. What is interesting about this approach to create colour is that there is great variability in the reflected colour by variation of the melanosome rod diameter and the cortex thickness. The arrangement is also different from the earlier mentioned case for peacocks, which have a square lattice arrangement and air spaces between the melanosomes in contrast to the ducks which have a hexagonal lattice and keratin between the melanosomes. Subsequent work [58] looking at similar 2D photonic hexagonally close packed melanosome arrays from wild turkeys (*Meleagris gallopavo*) and

violet-backed starlings (*Cinnyricinclus leucogaster*) showed that a further variation on this approach was to use hollow melanosomes. Therefore, rather than there being one scattering interface for the light there are now two as the hollow melanosomes behave as hollow cores with a thin shell.

4.2. Nucleation and growth type photonic structures (sphere structures)

A truly omnidirectional structural colour requires that the photonic structure be isotropic to give a wide viewing angle. To achieve this nature shifts to structures, which are far from perfect single crystal photonic structures, they exhibit some relative amount of disorder.

For simplicity, we begin with an examination of the sphere type structures found in turquoise blue Cotinga feathers. Whilst unable to visualise the size of the nano-features in a blue Cotinga feather [59] Mason was able to effectively extinguish the blue colour using the solvent ortho-cresol ($n \sim 1.54$) and so concluded one of the components was close to the solvent in refractive index, and the other is air. We now know these other domains were made from beta-keratin. Cutting edge TEM studies of the day were used to study the nanostructure of the purple-breasted Cotinga (*Cotinga cotinga*) [60] feather barbs. One of these TEM images from this work is shown in figure 9(a) along with a similar morphology found in the turquoise coloured plum-throated Cotinga (*Cotinga maynana*) [61].

Dyck examined the plum-throated Cotinga (*Cotinga maynana*), like the one shown in figure 9(b), and observed that the structure was made of spheroidal cavities distributed in a beta-keratin matrix [51]. The feather barbs do also contain a number of optically absorbing red carotenoids. Dyck goes on to summarise the literature in regards to the formation of these structures and argues that aggregation, like that seen for surfactants polymer mixtures, is somehow responsible for their formation. At later stages the coalescence of the sphere structure may possibly be the origin of the interconnected channel (spinodal) structures, however, based on the volume fraction

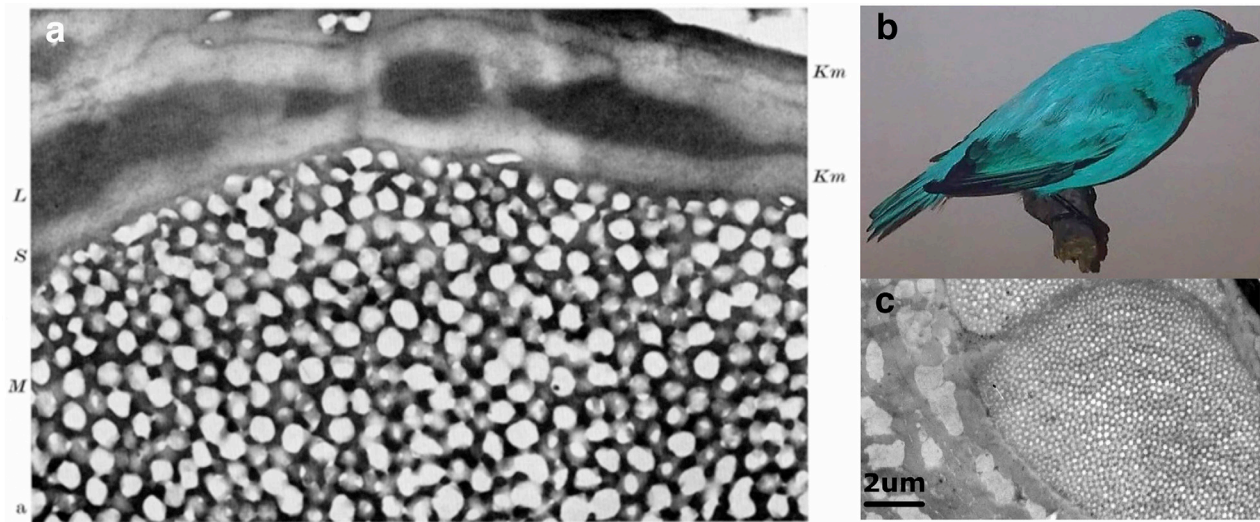


Figure 9. (a) TEM of the sphere structure found in the feather barbs of a purple-breasted Cotinga (*Cotinga cotinga*). [60] 1962 © Springer-Verlag 1962. With permission of Springer. (b) Plum-throated Cotinga (*Cotinga maynana*). This *Cotinga maynana* 1 image has been obtained by the authors from the Wikimedia website (https://commons.wikimedia.org/wiki/File:Cotinga_maynana_1.jpg), where it was made available by DenesFeri under a CC BY 4.0 licence. It is included within this article on that basis. It is attributed to Emőke Dénes. (c) Sphere categorised optical nanostructure measured using TEM for *Cotinga maynana*. Short-range order and near-field effects on optical scattering and structural coloration. Reproduced from [61]. CC BY 4.0.

of air in the spongy spinodal structures, which must be conserved, he later rules out the possibility of crossing from one morphology (sphere to spongy), and so these two structures must be distinct and have separate structure formation routes.

The observation by Prum *et al* [5] that feathers from the plum-throated Cotinga could be analysed as coherent Bragg reflectors altered the way in which we think of structural colour in many natural organisms such as birds, insects, beetles and butterflies. For a long time the origin of large number of blue structures found in the natural world had been thought to be due to Tyndall scattering structures or often called Tyndall blues. This was after the Irish physicist John Tyndall and the effect, which bears his name, and relates to the scattering of light from fine suspensions, smoke and colloidal particles. Prum *et al* [5] studied the optical nanostructure using electron microscopy of the feather barbs and observed that it was possible to use fast Fourier transform (FFT) image analysis to extract a dominant spatial lengthscale. This helped to pinpoint the light scattering mechanism as a kind of coherent reflection from an isotropic but nano-structured system, similar to the theory put forward by Benedek to understand the optical transparency of the eye [62]. As correlations in the structural arrangement of proteins in the lens and the cornea act to reduce the scattering as they do not occur independently [62]. These are then coherent reflectors.

A comprehensive study of caruncle tissue using FFT analysis of TEM images showed that there are many examples of animal tissue that are structurally coloured using the spherical structuring approach, with colours ranging from blue, green, orange and red [63]. An example of this type of optically structured collagen being the skin of the *Tragopan caboti*, like the specimen shown in figure 2(c). Other instances of the spherical morphology of structured collagen can be found in

the world of mammals, with well known examples being the striking features of the male mandrill (*Mandrillus sphinx*), which has a blue coloured face and a blue posterior [64].

We find this structural colour morphology consisting of spheroidal voids in a solid matrix in birds, odonata, mammals, and many other structurally coloured animals. It is this kind of universality highlights the great utility offered by this approach which we will discuss this more in the following sections.

4.3. Spinodal (spongy) photonic structures

The elegance of spinodal type structures comes from the mathematical appreciation of them; they are what are called self-similar structures. They are ubiquitous in nature from the cosmic scale down to the nanoscale and can readily be seen in phase separating mixtures. The location of spinodal quasi-ordered colour is in the barbs of feathers and not in the barbules. Gower examined in detail feather barbs in cross section for the bluebird (*Sialia sialis*) and the blue jay (*Cyanocitta cristata*) [65] finding that the blue colour region exists only the dorsal side. He also observed that a basal pigment layer was providing a way to maximise the colour, his light microscopy observations were obviously not able to measure or characterise the optical nanostructure. Some of the earliest work looking at feathers of the blue and yellow macaw (*Ara ararauna*) [60] used TEM imaging and saw a channel like morphology (we will use channel and spinodal interchangeably). Dyck also examined the blue feathers [51] of the peach-faced lovebird (*Agapornis roseicollis*) and using TEM and remarked that the optical structure is an irregular interconnected 3D network consisting of air and beta-keratin. This morphology Dyck described as comprising keratin rods

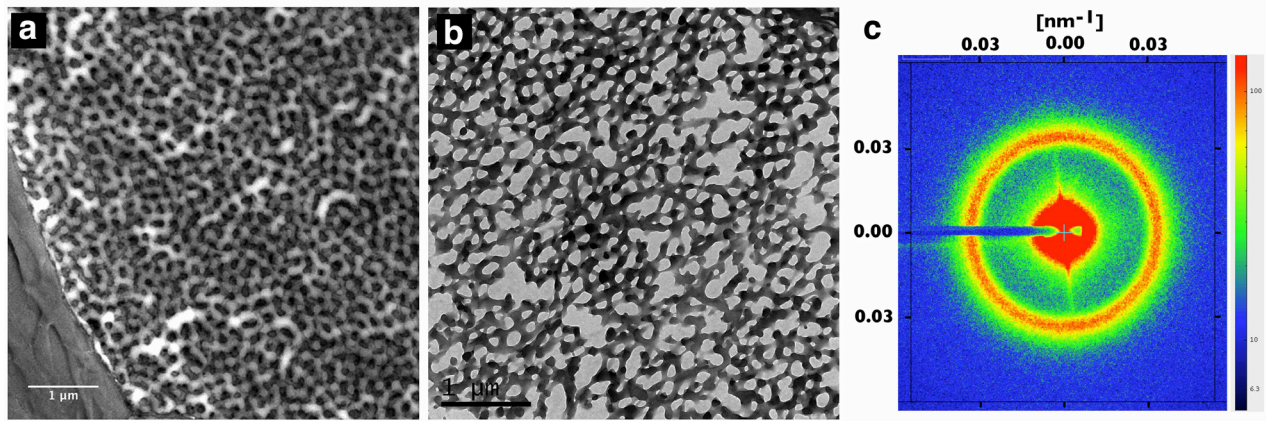


Figure 10. TEM images for two spinodal/spongy isotropic optical scattering nanostructures found in numerous bird feather barbs, (a) from the blue barb of a blue and yellow macaw (*Ara ararauna*), (b) from the barbs of a Eurasian jay feather (*Garrulus glandarius*) and (c) a SAXS pattern from the light blue feathers of a budgerigar (*Melopsittacus undulatus*).

~100 nm wide, and where they meet they leave an air void also ~100 nm in diameter, importantly no preferential orientation to the rods was observed in these measurements.

In 2009 Noh *et al* [66] put forward the hypothesis that birds were using the physics of phase separation and kinetic arrest to freeze in a particular domain spacing within a photonic structure. This enables birds to have the fine control over the structural colour of their feathers needed to give a range of structural colours. Their evidence was the striking similarity to the morphologies seen for binary blends of immiscible polymer mixtures [67]. This hypothesis is advantageous for birds as it allows them the possibility of tuning colour from the ultra-violet (UV) through the visible colour and into the infra-red (IR), simply by controlling the time phase separation is allowed to proceed, shorter time after the onset of phase separation gives smaller structures, whilst at later times the structure will have grown and the reflected light from these structures will be shifted to longer wavelengths.

Using SAXS to characterise the optical nanostructure Noh *et al* [68] compared the SAXS signal for the purple breasted Cotinga (*Cotinga cotinga*) and the Asian-fairy bluebird (*Irena puella*). These were categorised morphologically as sphere type and channel type structures respectively. Two examples of channel/spinodal nano-morphology can be seen in figure 10. The main difference structurally being that the sphere type (shown in figure 9) has much longer lengthscale correlations than the channel type, meaning that the spongy structure is more disordered. Their conclusion for both structures was that the isotropic arrangement of these structures makes their colour non-iridescent under natural light, i.e. they have no preferred orientation.

A comprehensive study of 230 bird species was performed by Saranathan *et al* [52] who again used the non-destructive technique of SAXS to compare the structures against their optical reflectance. By combining the two measurements they were able to infer the effective refractive index for the structure, n_{average} , by treating the system as a binary two phase system of air and beta keratin. They found good agreement between the shape and position of the SAXS scattering peak

on predicting the reflected optical hue and saturation. They were able to use SAXS to sort structures into sphere type or spongy/spinodal solely on the SAXS scattering pattern. Based on the large sample size studied they were able to conclude that non-iridescent structural colour from barb structuring with isotropic three-dimensional nanostructure, has evolved at least 44 times within 41 families across birds. This is important as it shows that the route chosen by nature to create these structures has converged on a solution that helps to give birds diversity in colour, but also uses a self-assembly route that is a minimal yet efficient solution to providing colour.

A paper from 2012 [69] by Yin *et al* studied in detail the non-iridescent blue of the scarlet macaw *Ara macao* and concluded that the structure could be modelled as a rod connected amorphous diamond like structure. They categorised it as a pseudo photonic bandgap, as there is not a complete photonic bandgap. With a mathematically simulated structure and using FDTD they saw strong agreement between with the microspectrometry measured reflectance. Importantly they were able to show that this structure only has long-range order, using other simulated volume filling fractions they could simulate reflectance. They saw that the 38% filling fraction is very close to the maximum from their optical modelling calculations.

5. Plant structural colour

We will mention a small number of structurally coloured plant systems, which have been increasingly studied in the last few years. A more thorough review can be found here [70]. An early study examining the self-assembly mechanism for colloidal like systems in *Selaginella* helped to explain the mechanism of depletion attraction as a process by which colloids accrete and order into closely packed regular structures. Where the depletion attraction process also requires the presence of a long chained macromolecule, like a polymer to become excluded from between the approaching colloids, osmosis withdraws the liquid from this space, helping to bring the particles closer together [71].

A study examining *Chondrus crispus* (Irish moss), a marine algae, concluded the mechanism responsible for producing the colour in the cuticles is due to a multilayer reflector structure. Interestingly this structure is highly porous, with water playing a vital role in the presentation and effectiveness of this reflected colour effect [72].

The interaction between plants and animals is an important part of a plants lifecycle in attracting pollinating insects. This was recently shown to be the case for a number of plants and in their relative attractiveness to bees [73] via the use of wrinkled like surfaces that result in scattered light with a strong angular dependence. It is possible to use self-assembly to create wrinkle and fold like surfaces in the laboratory, technologically these can improve the light harvesting in optical devices such as solar cells [74].

6. The physics of structural colour development

6.1. Current understanding of the mechanisms by which ridge reflectors develop in butterflies

The question of how complex ridge reflector structures form and then what are the developmental differences between butterfly species is as yet not fully understood. Existing work has demonstrated that the ridges form between longitudinal actin filaments, these are situated just below the scale surface and that they are in place prior to and maintained during optical ridge reflector development [75]. Presumably these provide the nascent scale with mechanical integrity and enable formation of the ridges whereby the cytoplasm protrudes outwards to form the ridge structures.

A study by Ghiradella [76] examined the very early stages of scale formation of a couple of butterfly species; the aim was to better understand how they produce the complex scale architecture. For this study the green olive hairstreak *Mitoura grynea* (*Lycaenidae: Theclinae*) and the blue spring azure (*Celastrina laden*) were used and their pupae were collected at certain narrowly spaced periods throughout the pupal period. They were fixed and subsequently stained using osmium tetroxide. Both species have similar surface morphology, having a small slender stalk (petiole) that is retained in place by the scale socket on the wing and the much larger featured blade. This is just essentially a flattened sac, comprised of a lower lamina, which faces the wing, and an exposed upper lamina, this is the surface that is shaped into a grid and comprises raised longitudinal ridges connected by thin cross-ribs. The pattern of ridges and ribs make a series of windows through which the interior lumen of the scale can be viewed. The development of the scale proceeds from a sheet structure where the ridges and the ridge spacing are just noticeable but they are in a highly contracted and collapsed form and have not achieved their spacing as yet. Later on (day 5) the ridges and cross ribs are much clearer and distinct with noticeable ridge lamellae, these are not straight and have strong curvature. In the following two to three days the scales straighten with the ridges and crossribs becoming much more distinct. Internally the structure of the developing photonic material has membrane-cuticle units that have a regular diameter, these

appear to be aggregating together. Membrane systems seem to be acting as guides for the developing structure.

Considerably less is known about what causes the folding of the ridges in order to produce the ridge lamellae optical elements. Ghiradella has suggested that they could be created by buckling of the nascent scale envelope by an outward applied mechanical stress and that the actin filaments may also be responsible for producing this stress. This would be in agreement with their very recent observations from Dinwiddle *et al* [77] who used fluorescence labelling of actin fibrils to show that they play a vital role in the process of cell elongation.

Ghiradella [36] suggested that the differences in architectural diversity must come about from comparatively small or slight modifications to the general basic non-specialised form. Each butterfly wing scale is made by a single cell, and results in a complex cuticular architecture, this structure is able to interact with light via structurally coloured features using lamellae ridge reflectors and also internal photonic scale crystal structuring to make components like the gyroid green reflecting structure.

A recent study demonstrated successful cell culture experiments of *Morpho peleides* cells, this approach may be a viable way in which to understand the very early stages of development of ridge reflectors [78]. Another technique which may prove important in future studies to understand this process may be the application of the gene editing technique of CRISPR/Cas9. This has already been used to switch off the presence of ommochrome pigment within certain regions of the wing for *Junonia coenia*, effectively altering the reflected colour, this was done by editing the *optix* gene, essentially a knockout of this gene [79].

6.2. The process of amphiphilic nano-templating of the inner scale crystal like structures in butterflies and beetle scales

A ground-breaking study by Ghiradella [76] showed that the bicontinuous, colour-producing, air-chitin nanostructures in the green wing scales of the butterfly *Mitoura gryneus*. This optical nanostructure develops from an initial template or pre-pattern, put in place by the smooth endoplasmic reticulum and cellular membrane into the central body of each individual wing-scale cell. Following the organization of the membrane pre-pattern, extra-cellular chitin is deposited into the lumen of this complex structure. After cell death, the remaining cytoplasmic spaces between the chitin become filled with air to create the strong refractive index difference that results in effective light scattering. This internal nanostructure within butterfly scales illustrates some of the subtle distinctions between nanostructural self-assembly and cellular physiological assembly.

These themes were further drawn on in the work by Saranatahn *et al* [80] where they characterised a large number of integumentary scales and setae. They saw a diversity in the kinds of structures which represents the richness of the phase diagram in volume fraction and domain sizes, which can be principally explained by the well known phase diagrams of amphiphilic molecules and block copolymers.

Wilts *et al* [81] examined the green scales of *Thecla opisena*, interestingly this has a gradient in the gyroid crystal size along the length of an individual scale. Using x-ray tomography they were able to ascertain that of the gyroid crystals they surveyed, the majority were single crystal domains. Importantly they do not share the same orientation, as would be required if a gyroid templating smooth endoplasmic reticulum was responsible for the patterning, it would need to itself be polycrystalline from the outset.

6.3. Spinodal structure growth and development

In this section we will try to understand the development and maturation of keratinocytes and how this leads to the fixed non-iridescent structural colour in the feather barbs. We shall begin by reviewing a study examining the early stages in development of the cells responsible for non-iridescent structural colour in bird feathers from Auber [82]. Developing feather germs were removed from an Indian pitta (*Pitta brachyuran*), see figure 11(a). In terms of the general morphology, the nascent ‘cloudy cells’ (responsible for the structural colour) have a polyhedral shape whereas cells not exhibiting this colour have a more spherical shape. A detailed examination of a transverse section of a turquoise *Pitta brachyuran* feather barb revealed the progression in vacuolization as the vacuole in the centre becomes more mature and the regions coalesce into a single vacuole. The perimeter region enclosing the vacuole is where the spongy nanostructure is located. The same progression in cell morphology was seen for a male blue dacnis (*Dacnis cayana*). This study did not have the necessary resolution to study the morphology of the photonic structure, a technique like TEM or high resolution SEM is needed to actually visualize this structure.

A variant on TEM called intermediate voltage TEM, capable of studying much thicker sample sections (250 nm–300 nm) was used to study the spongy layer optical nanostructure of the Eastern bluebird (*Sialia sialis*) [83]. This technique made it possible to probe the amorphous nanostructure and for the first time enable a full three-dimensional rendering of an amorphous photonic structure. Although the authors underscore that cross validation and comparison is needed with conventional SEM to corroborate the structure. The advantage of having a full 3D dataset is that it is possible to overcome some of the errors associated with 2D Fourier analysis by having successive slices in registry with one another, enabling a clearer understanding and allowing optical modelling of the reflected colour.

As mentioned before the blue and yellow macaw exhibit a spinodal like channel structure. Prum *et al* [84] used feathers of the *Ara ararauna* to examine the very early stages of newly growing feather germs and were able to begin to understand this process in much more detail. Using the spatial development and differences in maturation along a developing feather germ allowed them to use TEM to follow the different stages of cellular development. Sections were taken at distances from the base of the feather germ, in the range from 1 mm to 8.25 mm, where the feather germ was mature at 10 mm. Their

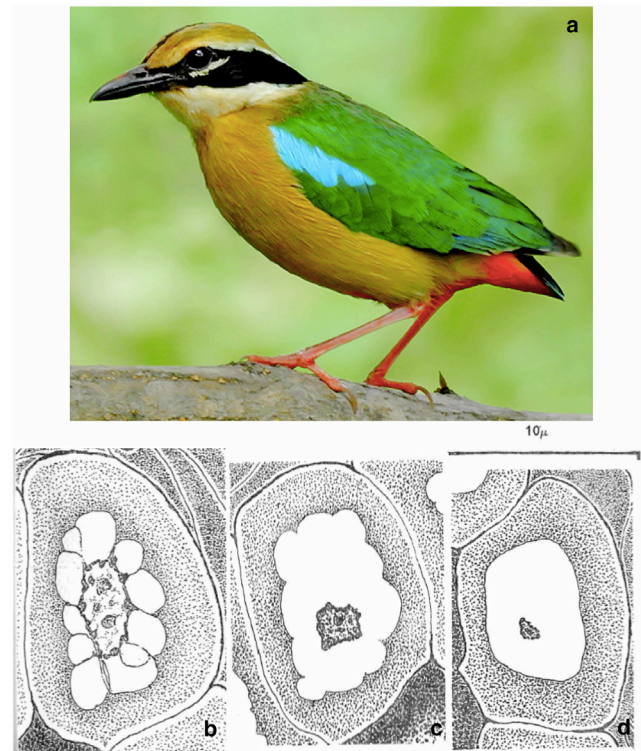


Figure 11. (a) Indian pitta (*Pitta brachyura*). This image has been obtained by the authors from the Wikimedia website ([https://commons.wikimedia.org/wiki/File:Indian_pitta_\(Pitta_brachyura\)_Photograph_by_Shantanu_Kuveskar.jpg](https://commons.wikimedia.org/wiki/File:Indian_pitta_(Pitta_brachyura)_Photograph_by_Shantanu_Kuveskar.jpg)) where it was made available by Shantanu Kuveskar under a **CC BY 4.0** licence. It is included within this article on that basis. It is attributed to Shantanu Kuveskar. (b)–(d) Hand drawn images of developing polyhedral cells going towards the final mature state in (d), with a fully developed vacuole. Reproduced by permission of The Royal Society of Edinburgh from [82].

first conclusion is that the colour develops within the medullary keratinocytes. They examined a number of different species confirmed as channel type and sphere type. At around a distance of 7 mm from the base of the feather germ they began to observe regions of patchy grey structure, these are regions having sufficient electron contrast and appear at the boundary of the medullary cell and the internal void. They found very few cells undergoing the intermediate stages, so this process must take place quite rapidly, possibly with a couple of hours. What they are definitive about is that during the formation of the spongy channel layer termed *keratinogenesis*, they could find no evidence for any intermediate cellular filaments, structuring proteins such as microtubules, the endoplasmic reticulum, or cell membrane, that would enable pre-patterning of the optical structure.

To understand further this process, they performed a structural analysis of the spongy keratin layer using Fourier analysis of the optical nanostructure measured using TEM. This enabled comparison with an evolving phase separating system validated to be undergoing spinodal decomposition. The model system was a phase separating mixture of polystyrene and polybutadiene temperature quenched and undergoing spinodal phase separation verified using light scattering to follow the evolution [85]. By normalizing the data in x and y

they were able to compare the shapes of the phase separated structures for both, the polymer blend and the spongy keratin. They saw good agreement in the shape of the peaks at higher spatial frequency, but at lower frequency they are hindered by artefacts from the TEM images. However, poor agreement was observed between the spinodally phase separating blend and the sphere morphology. The sphere feather data showed a secondary scattering peak in the region ~ 1.5 – 2 times that of the dominant peak k_{max} , making it possible to clearly differentiate between the two different morphology development processes of spinodal like structuring and nucleation and growth. From the electron microscopy images of the evolving medullary region it was possible to imply a mechanism of a pinned surface at the vacuole interface, followed by capillary flow of material and liquid. It was clear that these cells are essentially cut off from the dermal pulp of the feather germ. Whilst they are able to show a clear structural correlation between the spongy keratin structure in the medullary region of bird feather barbs and the spinodally decomposing polymer blend, they were not definitive about what causes the cessation of the phase separation process. This process must be precise and easily reproducible for it to freeze in the structure at a particular length scale needed to produce a certain colour, which is often highly conserved across species and is often a defining trait of the phenotype. They suggest that control of this process may be due to the irreversible polymerization of beta-keratin, which arrests the phase separation process.

Parnell *et al* [86] also used the technique of SAXS to study the distinctive alternating blue-white wing feathers from the Eurasian jay (*Garrulus glandarius*), previously studied using TEM by Schmidt and Ruska [60]. The SAXS beam used in this work had an x-ray beam size of $20\ \mu\text{m}$ by $20\ \mu\text{m}$, which enabled sampling of the feathers at specific points to pinpoint the colour. They also used SAXS to study a number of geographically diverse (Europe, South America and the Indian subcontinent) structurally coloured bird feathers. The analysis of the SAXS data and the resultant lengthscales are shown in figure 12. What they found was that the transitions in the optical structure are spatially well controlled along feathers and that the biological control mechanisms, which are as yet unknown, are able to reliably provide subtle, but measurable, changes in the structure and resulting structural colour with a small transition region. To ascertain more specific information about the transition between colours required the study of an individual feather barb.

This was performed using a single jay feather barb and is shown in figure 13. Here a point like x-ray beam was scanned along the single barb providing SAXS patterns which were analysed using correlation analysis to give the long period and the beta-keratin domain width as a function of barb position. In excellent agreement with the colour change along the barb they saw an oscillatory change in the optical nanostructure of beta-keratin and air, enabling the colour to be modulated from blue through to white in the periodic pattern that is seen on the wing feathers. The gaps correspond to the reduced x-ray contrast black regions where the colour is dominated by melanin pigment. What is clear is that the barb possesses lengthscales that span the complete range from $140\ \text{nm}$ – $210\ \text{nm}$ and the

only observable colours are blue and white respectively. This nicely showed the limitation on this structural colour production route and why the incorporation of optically absorbing pigments is important to give a diverse colour palette [15].

Using a dynamic scaling analysis [87] approach to plot all of the SAXS scattering data onto a master curve, it was possible to compare the shape of the scaled structure peaks for all points along the barb, shown in figure 13(e). Whilst the scaled scattering curves do not fully superpose and lie on top of each other to give strict self-similarity, they do not diverge far, and when compared with a spinodally phase separating blend of gelatin and dextran there is good agreement in their level of self-similarity [87].

It was possible to conclude that the process is not a one stage slow process, like polymerization of the beta-keratin which would effectively reduce the mobility in the system, but instead it must be a two stage process. This implies that freezing of the phase separation lengthscale and structure takes place on a time-scale that is separate in time and physically distinct from the time-scale characterizing the phase separation and coarsening process, and ultimately leads to the conclusion that this must be a two-stage process. This contrasts strongly with the prevailing school of thought that the phase separation process is halted by the competition between phase separation and the irreversible polymerization of beta-keratin, which provides no control over the final lengthscale [84].

We will now review some of the important physics regards spinodal phase separation and how this can be used to provide the kinds of morphologies we see. One of the first points to mention about spinodal phase separation is the universality of the structure factor, so no matter how long the phase separation has progressed it is possible to scale them numerically and they will have the same structure factor at all times.

Phase separation of a mixture occurs when a mixture moves from a stable region of the phase diagram into an unstable region. The two mechanisms of phase separation are spinodal decomposition and nucleation and growth. Spinodal decomposition occurs above the spinodal line when a mixture is unstable. In this region the diffusion coefficient is negative meaning that diffusion moves against the concentration gradient and from regions, which are depleted, to regions that are rich in a particular component.

In the metastable region phase separation occurs by nucleation and growth. In this region phase separation requires a large fluctuation in concentration to occur to create a nucleation site that can then increase in size. In a ‘real’ mixture it is uncommon for these large fluctuations to occur and instead nucleation sites are normally the result of impurities in the mixture, these impurities cause a large reduction in the energy required for nucleation. In nucleation and growth diffusion occurs with the concentration gradient from regions of high concentration to regions of low concentration and therefore the diffusion coefficient will be positive

Cahn [88] and Hilliard-Cook [89] are well known for their work on developing the theory of spinodal decomposition. In their work they considered a mixture which is free from defects and whose molar volume is independent of pressure and volume fraction which allowed the total Helmholtz free

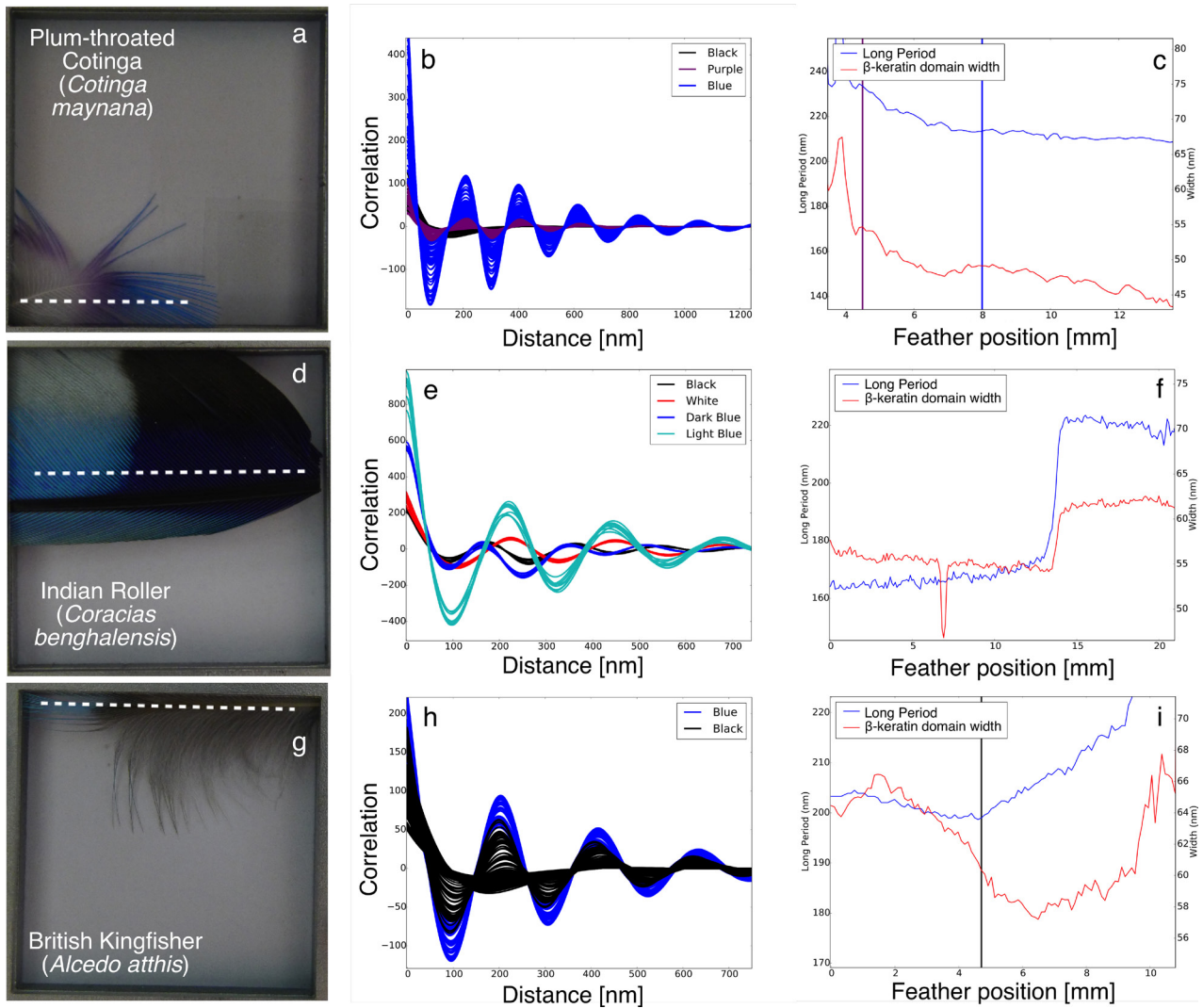


Figure 12. A geographical selection of bird feathers whose structural colour has been measured using SAXS and analysed using one dimensional correlation function analysis (ODCF). These include (a) the plum-throated Cotinga (*Cotinga maynana*), (d) the Indian roller (*Coracias benghalensis*) and (g) the British kingfisher (*Alcedo atthis*) along with the correlation functions (b), (e) and (h) using one dimensional correlation analysis, the y scale in (b), (e) and (h) is arbitrary, it is merely the extent of the correlation length in x that is important. In the right hand column is the ODCF derived long period and beta-keratin domain width for each species as a function of position (c), (f) and (i). Reproduced from [86]. CC BY 4.0.

energy to be written as a function of the local free energy, $f(\phi)$, and the gradient energy coefficient, κ , as given by equation (3). The diffusion of material within a mixture is driven by concentration gradients and the flux, J_1 , of component 1 and can be written in terms of the mobility, M , and the difference in the chemical potential, μ , as given by equation (4). The mobility term must be positive in order for phase separation to occur spontaneously

$$F = \int f(\phi) + \kappa \nabla^2 \phi dV \quad (3)$$

$$-J_1 = M \nabla (\mu_1 - \mu_2). \quad (4)$$

By assuming that κ is independent of concentration and neglecting the non-linear concentration term, it is possible to arrive at the final diffusion equation given by equation (5). This equation describes the rate of change of the volume fraction of a spinodally-phase separating mixture and is known as the Cahn–Hilliard equation

$$\frac{\partial \phi}{\partial t} = M \left(\frac{\partial^2 f}{\partial \phi^2} \right) \nabla^2 c - 2M\kappa \nabla^4 \phi. \quad (5)$$

One of the most important consequences of the Cahn–Hilliard theory is that it predicts a characteristic size of the domains of the developing (phase separating) microstructure. This characteristic size, Λ , is related to the local free energy through equation (6). In the late stage of phase separation, the domains will grow and coarsen to give the final microstructure, which is self-similar to the structure at earlier times. As discussed in earlier sections, the final spinodal microstructures are capable of producing broadband blue and white structural colours.

$$\Lambda = 2\pi \sqrt{-\frac{4\kappa}{\partial^2 f / \partial \phi^2}}. \quad (6)$$

At a particular temperature or when a non-solvent (coagulation bath) for the polymer is added to a molecularly dissolved polymer solution, the mixture transitions from the one-phase

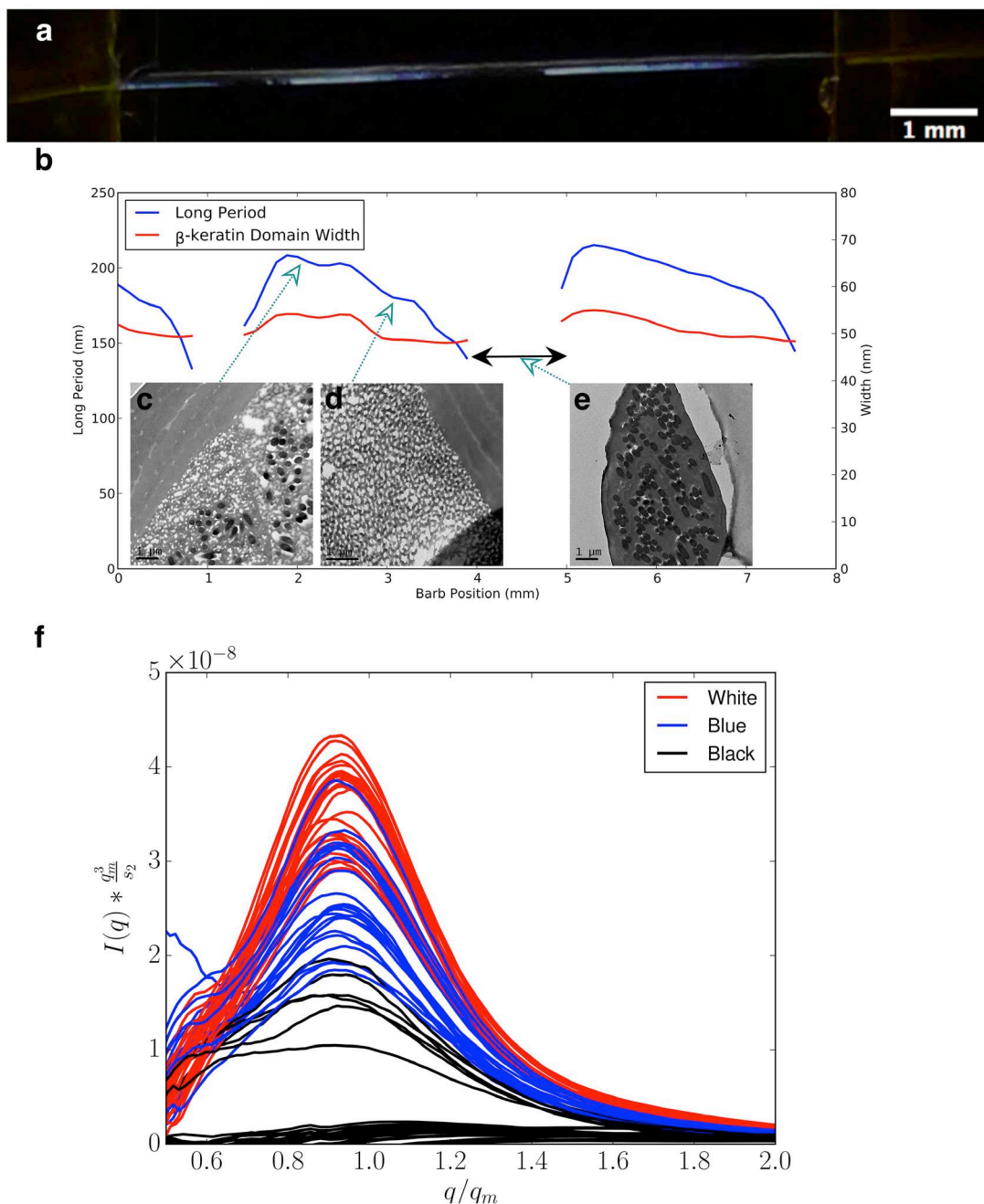


Figure 13. (a) The periodic variation in the jay feather structure and colour across a single feather barb. (b) The long period, which is the sum of neighbouring β -keratin and air domains. The SAXS signal was measured as a function of position across the single jay feather barb, and used one dimensional correlation analysis of the SAXS data. Electron microscopy (EM) images for the different coloured regions of the jay feather; (c) white region, (d) dark blue region and (e) the black region, where melanin creates the strong absorption of light and no clear β -keratin structure is observed in SAXS nor EM. (f) Dynamic scaling of the scattering data for the different regions of the feather barb. Reproduced from [86]. CC BY 4.0.

homogeneous region by crossing the binodal line to the two-phase region (see figure 14). This means that the initial mixed state is phase separating and can also be described as the unmixing of two immiscible liquids. This causes the formation of polymer-depleted and polymer-rich regions within the solution mixture. With continuing progress into the non-solvent quenching regime, either spinodal decomposition [90] or nucleation and growth processes take place, both of which are halted and frozen in by kinetic arrest at the Berghman’s point, where the glass transition temperature

of the polymer intersects the temperature of the system. The morphology achieved at this stage is the final fixed one observed experimentally.

To reiterate the process of liquid–liquid phase separation into a polymer-rich phase and a polymer-poor (depleted) phase happens when a critical concentration or threshold temperature is crossed, after which time the polymer becomes a better solvent for itself than the solvent it is dissolved or mixed in. This process is currently being explored to understand the ways in which many different biological and cellular processes take

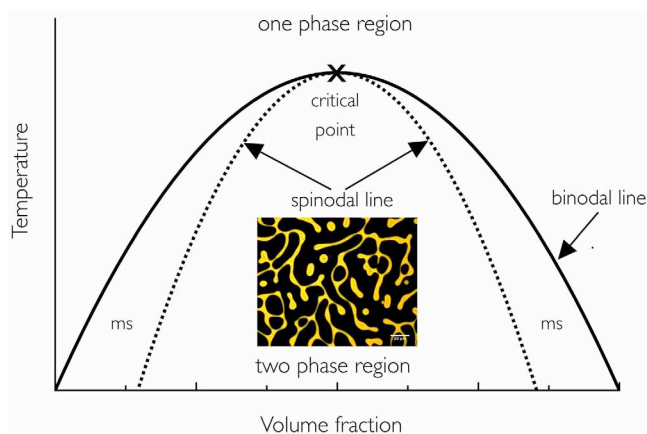


Figure 14. A phase diagram for a polymer solvent system showing the position of the binodal, separating the one phase region from the two-phase region. The (ms) metastable region lies between the binodal and the spinodal, and is where the quench is insufficient to access below the spinodal line, as such the phase separation will proceed via a nucleation and growth type mechanism. The inset image is for a polymer phase separated blend of poly(styrene) poly(3-hexylthiophene) made via spin coating.

place to organise and self-structure [91]. Defects in this process are providing new ways to explain a number of very serious and debilitating diseases. It is important to point out that the only way in which it is possible to definitively prove that the mechanism responsible for generating these spongy optical structures is a spinodal phase separation one, is to perform the same kind of scaling analysis on developing feather germs (also called feather pins). This would have to be carried out using immature developing feathers, where the adult feathers have a uniform colour, allowing the same kind of scaling analysis to be carried out and determine the degree of self-similarity as the feathers develop as a function of position which is effectively the time axis and phase separation time on the growing feather.

7. Conclusions

Do we observe similarities across the different species? And if so why is this the case? Is it such that the pattern formation mechanisms used to create these structures gives rise to similar morphology independent of the biopolymer used to create this optical effect.

We are now beginning to understand the morphologies responsible for structural colour in the natural world, we need not replicate them in their entirety but using optical modelling and simulations we can understand enough to derive the design principles. This makes it possible to stimulate new self-assembling photonic technologies using bioinspired design; from Bragg mirrors [92–94], butterfly surface structures [95, 96] and white structures [97].

Acknowledgments

AJP is grateful to the STFC funded European Synchrotron Radiation Facility in particular to the beamline ID02 and the assistance and support of Dr Sylvain Prevost which made possible the small angle x-ray scattering measurements presented

in this paper. We are indebted to Dr Alan Dunbar for regular access and use of a scanning electron microscope, purchased with support from grant EP/K001329/1 funded by the EPSRC. Some of this work was supported by the Technology Strategy Board, Innovate_UK (Grant Number 33692-239251). SLB is grateful for PhD funding from a University of Sheffield scholarship. Certain images in this publication have been obtained by the authors from the Wikipedia/Wikimedia website, where they were made available under a Creative Commons licence or stated to be in the public domain. Please see individual figure captions in this publication for details. To the extent that the law allows, IOP Publishing disclaim any liability that any person may suffer as a result of accessing, using or forwarding the images. Any reuse rights should be checked and permission should be sought if necessary from Wikipedia/Wikimedia and/or the copyright owner (as appropriate) before using or forwarding the images.

ORCID iDs

Andrew J Parnell  <https://orcid.org/0000-0001-8606-8644>

References

- [1] Srinivasarao M 1999 Nano-optics in the biological world: beetles, butterflies, birds, and moths *Chem. Rev.* **99** 1935–61
- [2] Vukusic P, Sambles J R and Lawrence C R 2000 Structural colour: colour mixing in wing scales of a butterfly *Nature* **404** 457
- [3] Vukusic P, Hallam B and Noyes J 2007 Brilliant whiteness in ultrathin beetle scales *Science* **315** 348
- [4] Parker A R, McPhedran R C, McKenzie D R, Botten L C and Nicorovici N P 2001 Aphrodite's iridescence *Nature* **409** 36–7
- [5] Prum R O, Torres R H, Williamson S and Dyck J 1998 Coherent light scattering by blue feather barbs *Nature* **396** 28–9
- [6] Hunt S, Bennett A, Cuthill I C and Griffiths R 1998 Blue tits are ultraviolet tits *Proc. R. Soc. B* **265** 451–5
- [7] Zi J, Yu X D, Li Y Z, Hu X H, Xu C, Wang X J, Liu X H and Fu R T 2003 Coloration strategies in peacock feathers *Proc. Natl Acad. Sci. USA* **100** 12576–8
- [8] Trismosin S 1531 *Splendor Solis (Splendor of the Sun)* (Augsburg)
- [9] Hooke R 1664 *Micrographia: Or Some Physiological Descriptions of Minute Bodies Made by Magnifying Glasses: With Observations and Inquiries Thereupon* (London: Jo. Martyn, and Ja. Allestry)
- [10] Bancroft W D 1924 Newton and the peacock *J. Phys. Chem.* **28** 351–9
- [11] Raman C V 1934 The origin of the colours in the plumage of birds *Proc. Indian Acad. Sci.* **1** 1–7
- [12] Fox D L 1976 *Animal Biochromes and Structural Colours: Physical, Chemical, Distributional & Physiological Features of Coloured Bodies in the Animal World* (Berkeley, CA: University of California Press)
- [13] Kinoshita S and Yoshioka S 2005 Structural colors in nature: the role of regularity and irregularity in the structure *ChemPhysChem* **6** 1442–59
- [14] Shawkey M D, Morehouse N I and Vukusic P 2009 A protean palette: colour materials and mixing in birds and butterflies *J. R. Soc. Interface* **6** S221–31
- [15] D'Alba L, Kieffer L and Shawkey M D 2012 Relative contributions of pigments and biophotonic nanostructures

- to natural color production: a case study in budgerigar (*Melopsittacus undulatus*) feathers *J. Exp. Zool.* **215** 1272–7
- [16] Stavenga D G, Tinbergen J, Leertouwer H L and Wilts B D 2011 Kingfisher feathers—colouration by pigments, spongy nanostructures and thin films *J. Exp. Zool.* **214** 3960–7
- [17] Tinbergen J, Wilts B D and Stavenga D G 2013 Spectral tuning of Amazon parrot feather coloration by psittacofulvin pigments and spongy structures *J. Exp. Biol.* **216** 4358–64
- [18] Leertouwer H L, Wilts B D and Stavenga D G 2011 Refractive index and dispersion of butterfly chitin and bird keratin measured by polarizing interference microscopy *Opt. Express* **19** 24061–6
- [19] Stavenga D G, Leertouwer H L, Piriš P and Wehling M F 2009 Imaging scatterometry of butterfly wing scales *Opt. Express* **17** 193–202
- [20] Vukusic P and Stavenga D G 2009 Physical methods for investigating structural colours in biological systems *J. R. Soc. Interface* **6** S133–48
- [21] Vukusic P and Sambles J R 2003 Photonic structures in biology *Nature* **424** 852–5
- [22] Sun J, Bhushan B and Tong J 2013 Structural coloration in nature *RSC Adv.* **3** 14862–89
- [23] Kinoshita S, Yoshioka S and Miyazaki J 2008 Physics of structural colors *Rep. Prog. Phys.* **71** 076401
- [24] Starkey T and Nanophotonics P V 2013 Light manipulation principles in biological photonic systems *Nanophotonics* **2** 289–307
- [25] Stavenga D G, Leertouwer H L, Meglič A, Drašlar K, Wehling M F, Piriš P and Belušić G 2018 Classical lepidopteran wing scale colouration in the giant butterfly-moth *Paysandisia archon* *PeerJ* **6** e4590
- [26] Ghiradella H, Aneshansley D, Eisner T, Silberglied R E and Hinton H E 1972 Ultraviolet reflection of a male butterfly: interference color caused by thin-layer elaboration of wing scales *Science* **178** 1214–7
- [27] Byrnes S J 2016 Multilayer optical calculations (arXiv:1603.02720)
- [28] Stavenga D G, Leertouwer H L and Wilts B D 2014 Coloration principles of nymphaline butterflies—thin films, melanin, ommochromes and wing scale stacking *J. Exp. Zool.* **217** 2171–80
- [29] Yoshioka S and Kinoshita S 2004 Wavelength-selective and anisotropic light-diffusing scale on the wing of the Morpho butterfly *Proc. R. Soc. B* **271** 581–7
- [30] Mason C W 1927 Structural colors in insects. II *J. Phys. Chem.* **31** 321–54
- [31] Vukusic P, Sambles J R, Lawrence C R and Wootton R J 1999 Quantified interference and diffraction in single Morpho butterfly scales *Proc. R. Soc. B* **266** 1403–11
- [32] Zhang S and Chen Y 2015 Nanofabrication and coloration study of artificial Morpho butterfly wings with aligned lamellae layers *Sci. Rep.* **5** 16637
- [33] Kolle M, Salgard-Cunha P M, Scherer M R J, Huang F, Vukusic P, Mahajan S, Baumberg J J and Steiner U 2010 Mimicking the colourful wing scale structure of the *Papilio blumei* butterfly *Nat. Nanotechnol.* **5** 511–5
- [34] Seago A E, Brady P, Vigneron J P and Schultz T D 2009 Gold bugs and beyond: a review of iridescence and structural colour mechanisms in beetles (Coleoptera) *J. R. Soc. Interface* **6** S165–84
- [35] Boden S A, Asadollahbaik A, Rutt H N and Bagnall D M 2011 Helium ion microscopy of Lepidoptera scales *Scanning* **34** 107–20
- [36] Ghiradella H 1985 Structure and development of iridescent Lepidopteran scales: the Papilionidae as a showcase family *Ann. Entomol. Soc. Am.* **78** 252–64
- [37] Ghiradella H and Radigan W 1976 Development of butterfly scales. II. Struts, lattices and surface tension *J. Morphol.* **150** 279–97
- [38] Poladian L, Wickham S, Lee K and Large M C J 2009 Iridescence from photonic crystals and its suppression in butterfly scales *J. R. Soc. Interface* **6** S233–42
- [39] Wilts B D, Michielsen K, De Raedt H and Stavenga D G 2012 Iridescence and spectral filtering of the gyroid-type photonic crystals in *Parides sesostris* wing scales *Interface Focus* **2** 681–7
- [40] Michielsen K and Stavenga D G 2008 Gyroid cuticular structures in butterfly wing scales: biological photonic crystals *J. R. Soc. Interface* **5** 85–94
- [41] Saranathan V, Osuji C O, Mochrie S G J, Noh H, Narayanan S, Sandy A, Dufresne E R and Prum R O 2010 Structure, function, and self-assembly of single network gyroid (I4132) photonic crystals in butterfly wing scales *Proc. Natl Acad. Sci. USA* **107** 11676–81
- [42] Gadov D H 1882 On the colour of feathers as affected by their structure *J. Zool.* **50** 409–22
- [43] Mason C W 1926 Structural colors in insects. I *J. Phys. Chem.* **30** 383–95
- [44] Dyck J 1979 Winter plumage of the rock ptarmigan: structure of the air-filled barbules and function of the white colour *Dansk. Orn. Foren. Tidsskr.* **73** 41–58
- [45] Hallam B T, Hiorns A G and Vukusic P 2009 Developing optical efficiency through optimized coating structure: biomimetic inspiration from white beetles *Appl. Opt.* **48** 3243–9
- [46] Luke S M, Hallam B T and Vukusic P 2010 Structural optimization for broadband scattering in several ultra-thin white beetle scales *Appl. Opt.* **49** 4246–54
- [47] Burrelli M, Cortese L, Pattelli L, Kolle M, Vukusic P, Wiersma D S, Steiner U and Vignolini S 2014 Bright-white beetle scales optimise multiple scattering of light *Sci. Rep.* **4** 6075
- [48] Cortese L, Pattelli L, Utel F, Vignolini S, Burrelli M and Wiersma D S 2015 Anisotropic light transport in white beetle scales *Adv. Opt. Mater.* **3** 1337–41
- [49] Wilts B D *et al* 2017 Evolutionary-optimized photonic network structure in white beetle wing scales *Adv. Mater.* **7** 1702057
- [50] Thomas D B, McGoverin C M, McGraw K J, James H F and Madden O 2013 Vibrational spectroscopic analyses of unique yellow feather pigments (spheniscins) in penguins *J. R. Soc. Interface* **10** 20121065
- [51] Dyck J 1971 Structure and colour-production of the blue barbs of *Agapornis roseicollis* and *Cotinga maynana* *Z. Zellforsch. Microsk. Anat. Histochem.* **115** 17–29
- [52] Saranathan V, Forster J D, Noh H, Liew S F, Mochrie S G J, Cao H, Dufresne E R and Prum R O 2012 Structure and optical function of amorphous photonic nanostructures from avian feather barbules: a comparative small angle x-ray scattering (SAXS) analysis of 230 bird species *J. R. Soc. Interface* **9** 2563–80
- [53] Mason C W 1923 Structural colors in feathers. II *J. Phys. Chem.* **27** 401–48
- [54] Yoshioka S and Kinoshita S 2002 Effect of macroscopic structure in iridescent color of the peacock feathers *Forma* **17** 161–81
- [55] Medina J M, Díaz J A and Vukusic P 2015 Classification of peacock feather reflectance using principal component analysis similarity factors from multispectral imaging data *Opt. Express* **23** 10198–212
- [56] Nakamura E, Yoshioka S and Kinoshita S 2008 Structural color of rock dove's neck feather *J. Phys. Soc. Japan* **77** 124801
- [57] Eliason C M and Shawkey M D 2012 A photonic heterostructure produces diverse iridescent colours in duck wing patches *J. R. Soc. Interface* **9** 2279–89
- [58] Eliason C M, Bitton P-P and Shawkey M D 2013 How hollow melanosomes affect iridescent colour production in birds *Proc. Biol. Sci.* **280** 20131505

- [59] Mason C W 1923 Structural colors in feathers. *I J. Phys. Chem.* **27** 201–51
- [60] Schmidt W J and Ruska H 1962 Tyndallblau-Struktur von Federn im Elektronenmikroskop *Z. Zellforsch. Microsk. Anat. Histochem.* **56** 693–708
- [61] Liew S F *et al* 2011 Short-range order and near-field effects on optical scattering and structural coloration *Opt. Express* **19** 8208–17
- [62] Benedek G B 1971 Theory of transparency of the eye *Appl. Opt.* **10** 459–73
- [63] Prum R O and Torres R H 2013 Fourier blues: structural coloration of biological tissues *Excursions in Harmonic Analysis* vol 2 pp 401–21 (Basel: Birkhäuser)
- [64] Prum R O 2004 Structural colouration of mammalian skin: convergent evolution of coherently scattering dermal collagen arrays *J. Exp. Zool.* **207** 2157–72
- [65] Gower C 1936 The cause of blue color as found in the bluebird (*Sialia sialis*) and the blue jay (*Cyanocitta cristata*) *Auk* **53** 178–85
- [66] Dufresne E R, Noh H, Saranathan V, Mochrie S G J, Cao H and Prum R O 2009 Self-assembly of amorphous biophotonic nanostructures by phase separation *Soft Matter* **5** 1792–5
- [67] Toolan D T W, Parnell A J, Topham P D and Howse J R 2013 Directed phase separation of PFO:PS blends during spin-coating using feedback controlled *in situ* stroboscopic fluorescence microscopy *J. Mater. Chem. A* **1** 3587
- [68] Noh H, Liew S-F, Saranathan V, Mochrie S G J, Prum R O, Dufresne E R and Cao H 2010 How noniridescent colors are generated by quasi-ordered structures of bird feathers *Adv. Mater.* **22** 2871–80
- [69] Yin H, Dong B, Liu X, Zhan T, Shi L, Zi J and Yablonovitch E 2012 Amorphous diamond-structured photonic crystal in the feather barbs of the scarlet macaw *Proc. Natl Acad. Sci. USA* **109** 10798–801
- [70] Vignolini S, Moyroud E, Glover B J and Steiner U 2013 Analysing photonic structures in plants *J. R. Soc. Interface* **10** 20130394
- [71] Hemsley A R, Collinson M E, Kovach W L, Vincent B and Williams T 1994 The role of self-assembly in biological systems: evidence from iridescent colloidal sporopollenin in Selaginella megaspore walls *Phil. Trans. R. Soc. Lond. B* **345** 163–73
- [72] Chandler C J, Wilts B D, Vignolini S, Brodie J, Steiner U, Rudall P J, Glover B J, Gregory T and Walker R H 2015 Structural colour in *Chondrus crispus* *Sci. Rep.* **5** 11645
- [73] Moyroud E *et al* 2017 Disorder in convergent floral nanostructures enhances signalling to bees *Nature* **550** 469–74
- [74] Kim J B, Kim P, Pégard N C, Oh S J, Kagan C R, Fleischer J W, Stone H A and Loo Y-L 2012 Wrinkles and deep folds as photonic structures in photovoltaics *Nat. Photon.* **6** 327–32
- [75] Greenstein M E 1972 The ultrastructure of developing wings in the giant silkworm, *Hyalophora cecropia*. II. Scale-forming and socket-forming cells *J. Morphol.* **136** 23–51
- [76] Ghiradella H 1989 Structure and development of iridescent butterfly scales: lattices and laminae *J. Morphol.* **202** 69–88
- [77] Dinwiddie A, Null R, Pizzano M, Chuong L, Krup A L, Tan H E and Patel N H 2014 Dynamics of F-actin prefigure the structure of butterfly wing scales *Dev. Biol.* **392** 404–18
- [78] Parker A R and Townley H E 2015 Making photonic structures via cell culture: morphobutterfly scales *Bioinspired Biomimetic Nanobiomater.* **4** 68–72
- [79] Zhang L, Mazo-Vargas A and Reed R D 2017 Single master regulatory gene coordinates the evolution and development of butterfly color and iridescence *Proc. Natl Acad. Sci. USA* **114** 10707–12
- [80] Saranathan V, Seago A E, Sandy A, Narayanan S, Mochrie S G J, Dufresne E R, Cao H, Osuji C O and Prum R O 2015 Structural diversity of arthropod biophotonic nanostructures spans amphiphilic phase-space *Nano Lett.* **15** 3735–42
- [81] Wilts B D, Apeleo Zubiri B, Klatt M A, Butz B, Fischer M G, Kelly S T, Spiecker E, Steiner U and Schröder-Turk G E 2017 Butterfly gyroid nanostructures as a time-frozen glimpse of intracellular membrane development *Sci. Adv.* **3** e1603119
- [82] Auber L 1974 Formation of ‘polyhedral’ cell cavities in cloudy media of bird feathers *Proc. R. Soc. Edinburgh B* **74** 27–41
- [83] Shawkey M D, Saranathan V, Pálsdóttir H, Crum J, Ellisman M H, Auer M and Prum R O 2009 Electron tomography, three-dimensional Fourier analysis and colour prediction of a three-dimensional amorphous biophotonic nanostructure *J. R. Soc. Interface* **6** S213–20
- [84] Prum R O, Dufresne E R, Quinn T and Waters K 2009 Development of colour-producing -keratin nanostructures in avian feather barbs *J. R. Soc. Interface* **6** S253–65
- [85] Takenaka M and Hashimoto T 1992 Scattering studies of self-assembling processes of polymer blends in spinodal decomposition. II. Temperature dependence *J. Chem. Phys.* **96** 6177–90
- [86] Parnell A J *et al* 2015 Spatially modulated structural colour in bird feathers *Sci. Rep.* **5** 18317
- [87] Tromp R H, Rennie A R and Jones R A L 1995 Kinetics of the simultaneous phase separation and gelation in solutions of dextran and gelatin *Macromolecules* **28** 4129–38
- [88] Cahn J W 1965 Phase separation by spinodal decomposition in isotropic systems *J. Chem. Phys.* **42** 93–9
- [89] Cook H E 1970 Brownian motion in spinodal decomposition *Acta Metall.* **18** 297–306
- [90] Binder K, Deutsch H P and Sariban A 1991 Monte Carlo studies of polymer interdiffusion and spinodal decomposition: a review *J. Non-Cryst. Solids* **131–3** 635–42
- [91] Gerlich D W 2017 Cell organization by liquid phase separation *Nat. Rev. Mol. Cell Biol.* **18** 593
- [92] Parnell A J, Tzokova N, Pryke A, Howse J R, Mykhaylyk O O, Ryan A J, Panine P and Fairclough J P A 2011 Shear ordered diblock copolymers with tuneable optical properties *Phys. Chem. Chem. Phys.* **13** 3179
- [93] Miyake G M, Piunova V A, Weitekamp R A and Grubbs R H 2012 Precisely tunable photonic crystals from rapidly self-assembling brush block copolymer blends *Angew. Chem., Int. Ed.* **51** 11246–8
- [94] Noro A, Tomita Y, Shinohara Y, Sageshima Y, Walish J J, Matsushita Y and Thomas E L 2014 Photonic block copolymer films swollen with an ionic liquid *Macromolecules* **47** 4103–9
- [95] Crne M, Sharma V, Blair J, Park J O, Summers C J and Srinivasarao M 2011 Biomimicry of optical microstructures of *Papilio palinurus* *Europhys. Lett.* **93** 14001
- [96] Srinivasarao M, Collings D, Philips A and Patel S 2001 Three-dimensionally ordered array of air bubbles in a polymer film *Science* **292** 79–83
- [97] Syurik J, Siddique R H, Dollmann A, Gomard G, Schneider M, Worgull M, Wiegand G and Hölscher H 2017 Bio-inspired, large scale, highly-scattering films for nanoparticle-alternative white surfaces *Sci. Rep.* **7** 46637